BMC Chemistry

RESEARCH Open Access

In silico drug evaluation by molecular docking, ADME studies and synthesis, characterization, biological activities, DFT, SAR analysis of the novel Mannich bases

Veysel Tahiroğlu[1*], Kenan Gören[2], Gül Kotan[3] and Haydar Yüksek[2]

Abstract

In this study, seven new Mannich bases **4a-g**, containing 1,2,4-triazole and 2,6-dimethylmorpholine were synthesized and characterized by ^{13}C-NMR, ^{1}H-NMR and IR spectroscopy. Newly synthesized compounds' antioxidant characteristics were assessed with three different techniques (Reducing Power, Metal Chelation Activity, and Free Radical Scavenging). These compounds were also evaluated for their antimicrobial activity against 6 different bacteria. In vitro studies revealed that the synthesized compounds exhibited high metal chelating activity due to the presence of -OH, C=O, -NR_2, and -O- groups, despite their low free radical scavenging and reducing activity. Furthermore, antibacterial tests revealed that compound **4e**, in particular, exhibited potent activity against six different bacterial species, demonstrating its potential as an antimicrobial agent. These results suggest that these compounds possess significant biological activities that may influence both metal ion chelating and microbial growth. These new Mannich bases were evaluated for their drug availability and absorption, distribution, metabolism, and excretion (ADME) properties using the SwissADME tool. ADME analysis results showed that the newly synthesized compounds could find application in the field focused on the production of effective and harmless pharmacological drugs. Molecular docking analysis was performed to investigate the potential Alzheimer's disease activities of the newly synthesized compounds with BChE (PDB: 6SAM) and GST (PDB: 5J41) enzymes. In molecular docking analysis, compound **4d** with enzyme 6SAM (docking score −9.91) and compound **4e** with enzyme 5J41 (docking score −8.37) among the synthesized compounds showed good results on potential Alzheimer's disease. In addition, SAR analysis was performed by calculating the HOMO-LUMO, ΔE values of the new compounds with DFT. SAR analysis results were compared with ADME, molecular docking analysis, and antimicrobial activity results. The high metal chelation and antimicrobial activities obtained in this study were consistent with the DFT-based HOMO-LUMO energy differences (ΔE) calculated from the electronic structures of the compounds. In particular, compounds with low energy differences exhibited both high binding affinity to target enzymes in molecular docking studies and effective results in biological assays, demonstrating a strong correlation between experimental findings and theoretical calculations. This consistency demonstrates

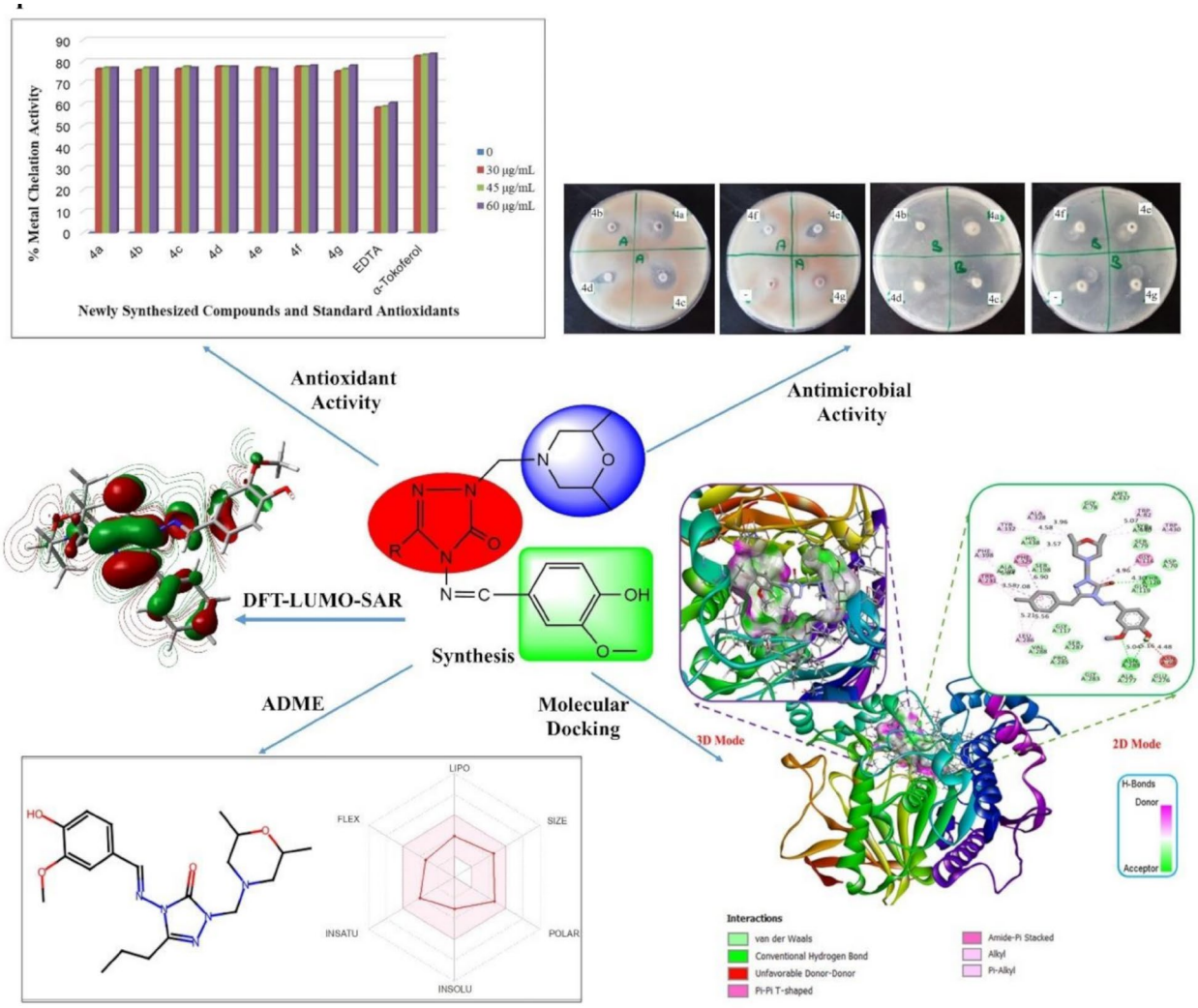
*Correspondence:
Veysel Tahiroğlu
veysel.tahiroglu@sirnak.edu.tr

Full list of author information is available at the end of the article

© The Author(s) 2025, corrected publication 2025. **Open Access** This article is licensed under a Creative Commons Attribution-NonCommercial-NoDerivatives 4.0 International License, which permits any non-commercial use, sharing, distribution and reproduction in any medium or format, as long as you give appropriate credit to the original author(s) and the source, provide a link to the Creative Commons licence, and indicate if you modified the licensed material. You do not have permission under this licence to share adapted material derived from this article or parts of it. The images or other third party material in this article are included in the article's Creative Commons licence, unless indicated otherwise in a credit line to the material. If material is not included in the article's Creative Commons licence and your intended use is not permitted by statutory regulation or exceeds the permitted use, you will need to obtain permission directly from the copyright holder. To view a copy of this licence, visit http://creativecommons.org/licenses/by-nc-nd/4.0/.

that the biological activities of compounds are directly related to their molecular electronic properties and that computational approaches can guide the design of effective compounds.

Graphical Abstract



Keywords Mannich bases, ADME, Antibacterial, Antioxidant, SAR, HOMO-LUMO

Introduction

Heterocyclic compounds are cyclic organic compounds that contain at least one heteroatom (usually nitrogen, oxygen, or sulfur) in addition to carbon atoms. These heteroatoms significantly influence the chemical and biological properties of the compound [1]. Heterocyclic structures are very common in both natural products and synthetic drugs and have important applications in many fields, including pharmaceuticals, agriculture, and materials science [2]. The chemical structure of heterocyclic compounds determines the molecule's reactivity, stability, and interaction with biological targets. For example, nitrogen-containing heterocyclic rings (such as imidazole, pyridine, and triazole) can bind to many biological targets and therefore play important roles in various biological activities, such as antiviral, antibacterial, antifungal, and anticancer [3]. Nitrogen-containing heterocyclic compounds, such as 1,2,4-Triazole, are widely used in antifungal and antiviral drugs. Investigating the various biological activities of these compounds is an important area of research in the development of new drug candidates [4]. Many heterocyclic compounds having 1,2,4-triazole rings have been linked to many biological activities, comprising antimicrobial, antioxidant, anticonvulsant, and antiviral effects [5, 6, 7, 8]. Mannich bases are used in medicinal chemistry, the paint

industry, cosmetics, synthetic polymers, petroleum and water purification products, etc [9, 10, 11]. Furthermore, the biological actions of Mannich bases include analgesic, antimycobacterial, antimicrobial, anti-inflammatory, antitumor, anticancer, and antifungal [12, 13, 14]. It has been decided to conduct important research to investigate the oxidative stress properties of antioxidants in organisms and cells. New chemicals have recently piqued the curiosity of scientists. Effective components that stop or lessen the effects of oxidative stress on cells can be found in natural sources [15, 16]. The human body and food system may create highly reactive free radicals, particularly oxygen-supplied radicals, through exogenous substances and endogenous metabolic processes. It oxidizes biomolecules, causing damage and death of cells. Oxidative damage is a major pathogenic factor in human disorders. For instance, oxidative damage has been linked to atherosclerosis, cancer, cirrhosis, emphysema, and arthritis [17]. Furthermore, overproduction of ROS (reactive oxygen species), which is brought on by a variety of stimuli and surpasses the antioxidant power of the human body, contributes to many pathophysiological procedures, including genotoxicity, diabetes, cancer, and inflammation [18]. Azole triazoles frequently used as antimicrobial drugs include fluconazole, itraconazole, terconazole, posaconazole, and voriconazole. However, other triazole drugs that can be considered are as follows: vorozole, letrozole, and anastrozole are used as non-steroidal drugs in cancer treatment; ribavirin is a nucleoside reverse transcriptase inhibitor and is a very effective antiviral agent, showing very serious effects on DNA and RNA viruses; rizatriptan is an antimigraine agent; trazodone is an antidepressant trapidyl hypotensive; benatradine, diuretic, and etoperidone are used as antidepressants [19]. Triazole systems are widely used, particularly in antifungal and antiviral therapies. Among the most well-known antimicrobial triazoles are fluconazole, itraconazole, terconazole, posaconazole, and voriconazole [20]. These antifungal diseases are effective in the treatment of these diseases and are widely preferred in clinical practice. Furthermore, nonsteroidal anti-inflammatory drugs (NSAIDs) with a triazole structure, such as vorozole, letrozole, and anastrozole, are used in the treatment of hormone-sensitive cancers and play a significant role in cancer treatment [21]. Ribavirin is a nucleoside transcriptase inhibitor effective against DNA and RNA viruses with broad-spectrum antiviral activity. Rizatriptan, used in migraine treatment, trazodone, known antidepressants, and benatradine and etoperidone, which possess diuretic and antidepressant properties, also belong to the triazole group. This study demonstrates the diversity of the triazole's chemical structure, the versatility of its application, and the potential for therapeutic potential of the drug [22].

Alzheimer's, a neurodegenerative disease, was first described by physician Alois Alzheimer in 1907. The disease took its name from the surname of this doctor [23, 24]. Alzheimer's illness is a growing, irreversible, lethal nervous system disease in which memory functions such as memory loss, speech disorders, orientation problems, inability to recognize people, difficulty in solving events, weaken over time, and the ability to perform daily self-care tasks decreases or even is completely forgotten over time [25, 26]. It is known that decreased cholinergic activity in Alzheimer's illness causes mental, functional, and behavioral disorders in patients. This phenomenon, known as the cholinergic hypothesis, is attempted to be overcome by raising the declining amount of acetylcholine neurotransmitter in the brain's synapses [27]. Cholinesterase enzymes are enzymes that hydrolyze the acetylcholine neurotransmitter in the synaptic region. Inhibition of these cholinesterase enzymes, AChE and BChE, increases the amount of acetylcholine, which increases cholinergic activity [28]. The FDA has authorized the use of tacrine, galantamine, rivastigmine, and donepezil compounds as AChE inhibitors for the cure of Alzheimer's illness. These inhibitors are the only licensed drugs used today [29].

Calculations utilizing density functional theory (DFT) have proven to be an important research tool for a variety of applications [30]. DFT calculations have progressed along two primary paths: the development of concepts about inhomogeneous fluids and phase transitions and the use of DFT calculations in multi-electronic systems in large-scale quantum chemistry [31]. Energy functional, spin, electric, magnetic, catalytic, chemical reactivity features, and intermolecular are all provided by DFT calculations [32, 33]. With the use of certain suitable quantum descriptors, like E_{LUMO}, energy gap, structure–activity relationships (SAR) enable an accurate connection with biological activity [34].

The rationale for this study is that various biological activities (antimicrobial, antioxidant) of heterocyclic compounds containing 1,2,4-triazole rings have been widely reported. Furthermore, the significant applications of Mannich bases in medical and industrial fields and their numerous biological effects necessitate their synthesis and study. The fact that damage caused by oxidative stress in organisms and cells is a fundamental cause of many diseases, and that decreased cholinergic activity plays a critical role in the course of disease, particularly in neurodegenerative diseases such as Alzheimer's, motivates our study. Therefore, the need to develop cholinesterase enzyme inhibitors is crucial. Furthermore, considering the importance of computational chemistry (DFT) and molecular docking analyses for predicting the biological activity of new compounds and understanding their structure-activity relationships, the fundamental

rationale for our research is to evaluate our synthesized Mannich bases using these methods.

Experimental

Materials and reagents

The necessary chemical compounds were obtained from Aldrich, Merck AG and Fluka. ^{1}H and ^{13}C-NMR spectra used to elucidate the structures of the synthesized compounds were obtained with a Bruker Ultrashield Plus Biospin spectrometer at 400 MHz and 100 MHz, respectively, in DMSO-d6 with TMS as internal standard. An Alpha-P Bruker FT-IR spectrometer was used for IR spectra. A Stuart SMP30 melting point apparatus was used to determine melting points. UV absorption spectra were measured in 10 mm quartz cells between 562 and 700 nm using a PG Instruments Ltd T80 UV/Vis spectrometer. Microsoft Excel 97-2003 application was used to generate antioxidant activity graphs. ChemDraw 22 tool was used to draw the synthesis scheme of the synthesized molecules. Schrödinger's Maestro Molecular Modeling platform [35] was used to investigate the exact binding site and binding process of ligand-protein interactions. Molecular docking study were visualized with Discovery Studio 2016 client [36]. ADME analysis was performed using the SwissADME web tool [37]. Gaussian 09 [38] program was used for SAR analysis. The following strains of bacteria and yeast were all acquired from Microbiological Environmental Protection Laboratories (France): the Bacillus cereus ATCC-12,767, Bacillus subtilis ATCC-12,764, Klebsiella pneumonia ATCC-4454, Pseudomonas aeruginosa ATCC-26,944, Escherichia coli ATCC-26,834, and Staphylococcus aureus ATCC-5649.

General procedure for synthesis of 1-(2,6-dimethylmorpholin-4-yl-methyl)-3-alkyl(aryl)-4-(3-methoxy-4-hydroxybenzylideneamino)-4,5-dihydro-1*H*-1,2,4-triazole-5-one (4)

0.01 mol **3**(**a**-**g**) substances were dissolved in 0.1 L ethanol. The prepared solution was added to 0.01 mol 2,6-dimethylmorpholine and 35% 0.03 mol formaldehyde solution, stirred for 3 h, and left to precipitate in the freezer at -17 °C. The precipitated crude substance was filtered and cleaned with chilly alcohol. The product raw material was crystallized several times with ethanol. After being vacuum-dried, these crystals were recognized as molecules **4**(**a**-**g**).

4a: M.P. 122 °C, Yield 89%, IR: 3500 (OH), 1692 (C = O), 1593 (C = N), 864 and 814 (1,2,4-trisubstituted benzene ring) cm^{-1}; ^{1}H-NMR (DMSO-d_6, δ): [1.03 (d; J = 6,4 0 Hz), 1.11 (d; J = 6,40 Hz)] (6 H, 2CH_3), [2.01 (t, J = 10.80 Hz), 2.26–2.29 (m), 2.74 (d, J = 11.20 Hz), 2.76 (d, J = 11.20 Hz), 3.51–3.54 (m), 3.83 (m)] (Morpholine H), 2.29 (s, 3 H, CH_3), 3.83 (s, 3 H, OCH_3), 4.53 (s, 2 H, NCH_2N), [6.90 (d, 1H; J = 8.00 Hz), 7.26 (d, 1H; J = 8.00 Hz), 7.28 (s, 1H)] (ArH), 9.49 (s, 1H, N = CH); ^{13}C-NMR (DMSO-d_6, δ): 11.01 (CH_3), 17.89 and 18.93 2CH_3, [55.03 and 55.61 2CH_2, 71.03 2CH] (Morpholine C), 55.64 OCH_3, 65.40-65.55 NCH_2N, [110.39 (CH), 115.66 (CH), 122.71 (CH), 124.50 (C), 142.96 (C) 150.37 (C)] (ArC), 143.00 (Triazol C_3), 150.36 (Triazol C_5), 155.33 (N = CH).

4b: M.P. 173 °C, Yield 87%, IR: 3074 (OH), 1698 (C = O), 1587 (C = N), 862 and 828 (1,2,4-trisubstituted benzene ring) cm^{-1}; ^{1}H-NMR (DMSO-d_6, δ): 0.96 (t, 3 H, $CH_2CH_2CH_3$; J = 7.260 Hz), 1.71 (sext, 2 H, $CH_2CH_2CH_3$; J = 7.20 Hz), [1.03 (d; J = 6,00 Hz), 1.11 (d; J = 6,40 Hz)] (6 H, 2CH_3), [2.02 (t, J = 10.08 Hz), 2.26–2.30 (m), 2.51 (m), 2.76 (d, J = 10.40 Hz), 3.51–3.54 (m), 3.83–3.88 (m)] (Morpholine H), 2.65 (t; 2 H, $CH_2CH_2CH_3$ J = 7.20 Hz), 3.83 (s, 3 H, OCH_3), 4.55 (s, 2 H, NCH_2N), [6.90 (d, 1H; J = 8.00 Hz), 7.26 (d, 1H; J = 1.60 Hz), 7.28 (s, 1H)] (ArH), 9.49 (s, 1H, N = CH); ^{13}C-NMR (DMSO-d_6, δ): 13.34 ($CH_2CH_2CH_3$), 17.80 and 18.92 2CH_3, 18.92 ($CH_2CH_2CH_3$), 26.92 ($CH_2CH_2CH_3$), [55.06–55.61 (2CH_2), 71.01 (2CH)] (Morpholine C), 55.66 OCH_3, 65.40-66.14 NCH_2N, [110.40 (CH), 115.71 (CH), 122.53 (CH), 124.61 (C), 146.04 (C) 150.35 (C)] (ArC), 145.54 (Triazol C_3), 150.45 (Triazol C_5), 155.30 (N = CH).

4c: M.P. 180 °C, Yield 87%, IR: 3027 (OH), 1702 (C = O), 1585 (C = N), 864 and 828 (1,2,4-trisubstituted benzene ring), 738 and 704 (monosubstituted benzene ring) cm^{-1}; ^{1}H-NMR (DMSO-d_6, δ): [1.03 (d; J = 6,40 Hz), 1.11 (d; J = 6,40 Hz)] (6 H, 2CH_3), [2.00 (t; J = 10.80 Hz), 2.49–2.51 (m), 2.77 (d; J = 10.40 Hz), 3.51–3.53 (m), 3.55–3.83 (m)] (Morpholine H), 3.83 (s, 3 H, OCH_3), 4.07 (s, 2 H, CH_2Ph), 4.58 (s, 2 H, NCH_2N), [6.86 (d, 1H; J = 8.00 Hz), 7.18 (dd, 1H; J = 2.00 Hz), 7.21–7.24 (m, 1H), 7.30 (d, 1H; J = 4.40 Hz), 7.31–7.35 (m, 4 H)] (ArH), 9.46 (s, 1H, N = CH); ^{13}C-NMR (DMSO-d_6, δ): 17.89 and 18.85 2CH_3, 31.01 (CH_2Ph), [55.00-55.56 (2CH_2), 71.01 (2CH)] (Morpholine C), 55.68 OCH_3, 65.41–66.27 NCH_2N, [109.66 (CH), 115.58 (CH), 123.10 (CH), 124.89 (C), 148.07 (C) 150.34 (C)] (ArC), 144.03 (Triazol C_3), 150.40 (Triazol C_5), 154.82 (N = CH).

4d: M.P. 143 °C, Yield 78%, IR: 3023 (OH), 1702 (C = O), 1593 (C = N), 868 and 802 (1,2,4-trisubstituted benzene ring), 802 (1,4-disubstituted benzene ring) cm^{-1}; ^{1}H-NMR (DMSO-d_6, δ): [1.03 (d; J = 6,00 Hz), 1.12 (d; J = 6,40 Hz)] (6 H, 2CH_3), [1.98 (t, J = 1.60 Hz), 2.27–2.49 (m), 2.50–2.51 (m), 2.76 (d, J = 10.40 Hz), 3.51–3.55 (m)] (Morpholine H), 2.24 (s, 3 H, CH_3Ph), 3.83 (s, 3 H, OCH_3), 4.01 (s, 2 H, CH_2Ph), 4.57 (s, 2 H, NCH_2N), [6.88 (d, 1H; J = 8.00 Hz), 7.11 (d, 2 H; J = 8.00 Hz), 7.19 (d, 1H), 7.21 (d, 2 H; J = 2.00 Hz), 7.35 (s,1H)] (ArH), 9.46 (s, 1H, N = CH); ^{13}C-NMR (DMSO-d_6, δ): 17.03 and 18.05 2CH_3, 20.56 (CH_3Ph), 30.60 (CH_2Ph), [55.08 (2CH_2), 55.54 (2CH_2), 71.01 (2CH)] (Morpholine C), 55.69 OCH_3, 65.40-66.24 NCH_2N, [109.65 (CH), 115.41 (CH), 122.69

(CH), 124.62 (C), 147.01 (C) 150.40 (C)] (ArC), 144.98 (Triazol C_3), 150.32 (Triazol C_5), 154.44 (N = CH).

4e: M.P. 172 °C, Yield 74%, IR: 2970 (OH), 1701 (C = O), 1587 (C = N), 859 and 818 (1,2,4-trisubstituted benzene ring), 818 (1,4-disubstituted benzene ring) cm^{-1}; ^{1}H-NMR (DMSO-d_6, δ): [1.06 (d; J = 6,00 Hz), 1.12 (d; J = 6,40 Hz)] (6 H, $2CH_3$), [1.99 (t; J = 1.60 Hz), 2.51–2.52 (m), 2.77 (d; J = 10.40 Hz), 3.51–3.55 (m)] (Morpholine H), 3.70 and 3.86 (s, 3 H, OCH_3), 4.01 (s, 2 H, CH_2Ph), 4.58 (s, 2 H, NCH_2N), [6.91 (d, 2 H; J = 8.00 Hz), 7.22 (d, 1H; J = 2.00 Hz), 7.23 (dd, 1H; J = 6.40 Hz), 7.24 (d, 2 H; J = 1.60 Hz), 7. 28 (d, 1H; J = 8.40 Hz),] (ArH), 9.49 (s, 1H, N = CH); ^{13}C-NMR (DMSO-d_6, δ): 17.80 and 18.82 $2CH_3$, 30.23 (CH_2Ph), [55.55 ($2CH_2$), 55.70 ($2CH_2$), 71.02 (2CH)] (Morpholine C), 55.09 and 56.05 (OCH_3), 65.42–67.21 NCH_2N, [109.70 (CH), 113.86 (CH), 122.61 (CH), 124.65 (C), 146.44 (C) 150.45 (C)] (ArC), 144.98 (Triazol C_3), 150.41 (Triazol C_5), 154.44 (N = CH).

4f: M.P. 105 °C, Yield 88%, IR: 3050 (OH), 1704 (C = O), 1584 (C = N), 861 and 806 (1,2,4-trisubstituted benzene ring), 806 (1,4-disubstituted benzene ring) cm^{-1}; ^{1}H-NMR (DMSO-d_6, δ): [1.03 (d; J = 6,40 Hz), 1.11 (d; J = 6,40 Hz)] (6 H, $2CH_3$), [1.99 (t; J = 4.40 Hz), 2.50–2.51 (m), 2.77 (d; J = 10.40 Hz), 3.50–3.54 (m), 3.84 (m)] (Morpholine H), 3.83 (s, 3 H, OCH_3), 4.57 (s, 2 H, NCH_2N), [6.88 (d, 1H; J = 8.00 Hz), 7.20 (d, 1H; J = 6.40 Hz), 7.31 (s, 1H), 7.32–7.39 (m, 4 H)] (ArH), 9.47 (s, 1H, N = CH); ^{13}C-NMR (DMSO-d_6, δ): 17.80 and 18.85 $2CH_3$, 30.41 (CH_2Ph), [55.05 ($2CH_2$), 55.66 ($2CH_2$), 71.01 (2CH)] (Morpholine C), 55.57 (OCH_3), 65.41–66.31 NCH_2N, [109.70 (CH), 113.86 (CH), 122.61 (CH), 124.65 (C), 146.44 (C) 148.08 (C)] (ArC), 144.98 (Triazol C_3), 150.39 (Triazol C_5), 154.66 (N = CH).

4 g: M.P. 180 °C, Yield 87%, IR: 3048 (OH), 1703 (C = O), 1589 (C = N), 887 and 826 (1,2,4-trisubstituted benzene ring), 746 and 687 (monosubstituted benzene ring) cm^{-1}; ^{1}H-NMR (DMSO-d_6, δ): [1.03 (d; J = 4,40 Hz), 1.13 (d; J = 6,40 Hz)] (6 H, $2CH_3$), [2.09 (t; J = 10.80 Hz), 2.50–2.51 (m), 2.83 (d; J = 10.40 Hz), 3.54–3.58 (m)] (Morpholine H), 3.81 (s, 3 H, OCH_3), 4.69 (s, 2 H, NCH_2N), [6.91 (d, 1H; J = 8.00 Hz), 7.27 (d, 1H; J = 6.80 Hz), 7.29 (s, 1H), 7.39–7.40 (m, 4 H)] (ArH), 9.43 (s, 1H, N = CH); ^{13}C-NMR (DMSO-d_6, δ): 17.89 and 18.92 $2CH_3$, [55.01 ($2CH_2$), 55.59 ($2CH_2$), 71.07 (2CH)] (Morpholine C), 55.52 (OCH_3), 65.43–66.70 NCH_2N, [110.39 (CH), 115.72 (CH), 122.87 (CH), 124.44 (C), 148.08 (C) 149.85 (C)] (ArC), 143.09 (Triazol C_3), 150.59 (Triazol C_5), 158.18 (N = CH).

Antioxidant activity

Reducing power

Utilizing the Oyaizu technique, the reducing power was determined [39]. The synthesized molecules' reducing abilities were evaluated by the degree of transformed of the Fe^{3+} ferricyanide complex to the Fe^{2+}/ferrous state [40]. Samples in solutions with varying amounts (100-250-500 µg/mL) prepared in dimethylsulfoxide (1 mL) were mixed with 2.5 mL potassium ferricyanide, and phosphate buffer. Once the test tubes were carefully mixed, they were incubated for 15 min at 40 °C. Following incubation, every test tube was brought to room temperature, and 2.5 mL TCA solution was added. After that, the test tubes were centrifuged for 15 min at 3000 pm. 2.5 Milliliters of the filtrate were removed and put into test tubes. The mixture was then mixed with 2.5 water and 0.5 milliliters $FeCl_3$ solution. The resulting colored complexes were detected with a UV spectrophotometer at 700 nm.

Free radical scavenging activity

The free radical scavenging activities of the newly synthesized molecules were characterized based on the DPPH radical scavenging model and the Blois technique [41, 42]. The DPPH radical scavenging model is a commonly utilized method to assessment of antioxidant activity when contrasted with alternative antioxidants [43]. It was thought that the way antioxidants affected DPPH radical scavenging was because of their ability to donate hydrogen [44]. The sample mixtures at various concentrations in DMSO were mixed with 0.1 mM DPPH solution in ethanol. The test tubes were mixed thoroughly and then kept for 20 min at room temperature, and their absorbance was determined with UV spectrophotometer.

Metal chelate activity

The ions and the standards' chelation impact on compounds was examined. Ferrozine could form quantitative compounds with Fe^{2+}. Chelation agents cause disruptions in the production of complexes, which lower the complex's color hue [45]. Consequently, color reduction testing may be used to assess the chelation activity of the coexisting chelator. In living things, transition metals play an important part in the generation of free oxygen radicals [46]. Ferric iron (Fe^{3+}) is a biologically comparatively passive type of iron. However, depending on the conditions, especially pH, it could be reduced to active Fe^{2+} and oxidized back by Haber-Weiss processes with Fenton-type reactions or superoxide anions with the production of the hydroxyl radical [47]. The production of these radicals can lead to DNA damage, lipid peroxidation, and protein modification. Chelating agents can obstruct metal-dependent processes by failing to activate metal ions [48].

Metal chelate activity determination was made using the Dinis method [49]. Briefly, samples and standards placed in test tubes were diluted using purified water to complete concentrations of 30, 45, and 60 µg/mL to a total volume of 200 µL. Then, $FeCl_2.4H_2O$, ethyl alcohol,

and ferrozine were mixed by adding and left at room temperature for 10 min. The outcome's color was read against blank (other than ferrozine) on a UV spectrophotometer at 562 nm.

Antimicrobial activity

Antimicrobial properties of molecules synthesized using agar well diffusion technique were determined [50]. To prepare 1 mg/ml extract stock solution, newly synthesized molecules were weighed and dissolved in dimethylsulfoxide. Each microorganism was diluted to 106 colony-forming units (CFU) per milliliter by suspending it in Mueller-Hinton Broth. A "flood inoculum" was applied to the surface of Mueller Hinton Agar and then dried. Utilizing a sterile cork borer, wells of 5 millimeters in diameter were removed from the agar and filled with a chemical material ranging from 250 to 5000 µg/50 µl. The plates were incubated for 18 h at 35 °C. By assessing the zone of inhibition against the test organism, antimicrobial activity was assessed. Positive controls included ampicillin (10 µg) for streptomycin bacteria and fluconazole (5 µg) for yeasts, and DMSO was utilized as a solvent control.

DFT study

Density Functional Theory (DFT) is a powerful quantum chemistry method widely used to predict the electronic structures of organic and biologically active compounds [51]. Especially in drug design, the frontier molecular orbital (HOMO and LUMO) energy values obtained by DFT are critical in predicting the reactivity of a compound and its interaction with biological targets. The HOMO energy level represents the electron donating (nucleophilic) capacity of the compound, while the LUMO energy level indicates its electron accepting (electrophilic) potential. Higher EHOMO values facilitate the compound's electron donation to vacant orbitals on the target receptor, while lower ELUMO values increase the molecule's electron accepting tendency [52]. In this study, geometric optimizations of target compounds **4**(**a**–**g**) were performed in the Gaussian 09 program [38] using the B3LYP [34] functional of DFT and the 6-311G(d, p) [53] basis set. Parametric data such as HOMO-LUMO energy levels, total energy, and molecular volume were obtained through theoretical calculations. These data were evaluated in the context of the structure-activity relationships (SAR) of the compounds, and the results were compared with ADME profiles, molecular docking analyses, and antimicrobial activity data. Thus, the extent to which theoretical calculations were consistent with experimental data was analyzed. This holistic approach provided by DFT in predicting molecular properties is invaluable in identifying potential lead compounds in the drug discovery process.

Molecular docking studies

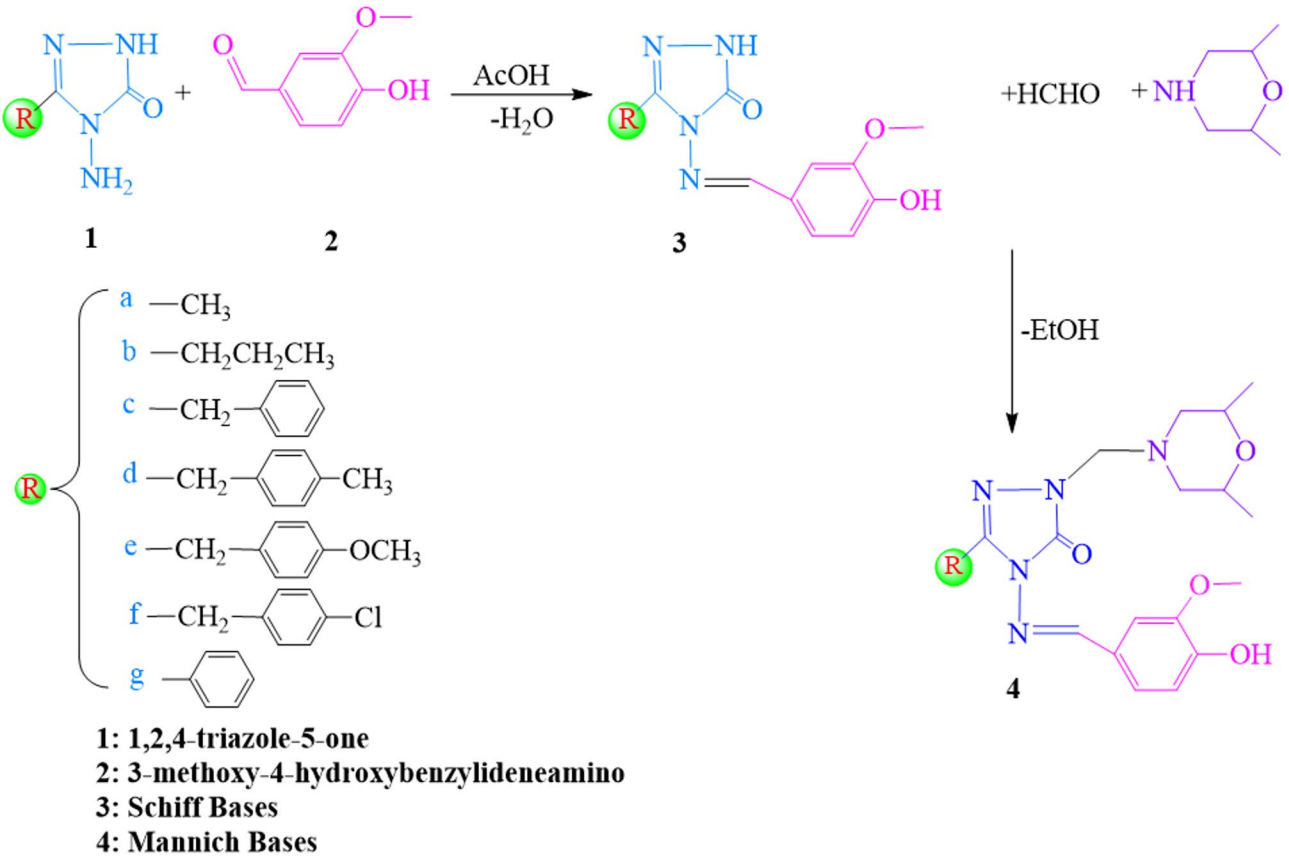
For docking analysis, the crystal structures of GST (PDB: 5J41) and Butyrylcholinesterase (BChE) (PDB: 6SAM) were downloaded using the Protein Data Bank [54]. To determine the specific binding site and binding mechanism of the ligand on the target protein, molecular docking studies were performed using the Maestro Molecular Modeling platform (version 11.8) [35] developed by Schrödinger, LLC. In the first stage of the study, the protein crystal structure was optimized using the Protein Preparation Wizard module to model the system accurately. During this process, all water molecules in the crystal structure were removed, missing hydrogen atoms on the protein were completed, and the protein was structurally stabilized by providing appropriate ionization states. To ensure more realistic docking results, the active binding site of the protein was defined to be flexible. Following this, the receptor grid generation stage was initiated, and structures called "network boxes" were used for this purpose. These boxes created three-dimensional networks at protein binding sites, enabling flexible docking strategies and enabling more accurate representation of the binding site. Ligand conformations obtained from the molecular docking process were evaluated based on their binding energies, and the conformation with the lowest binding energy was considered the conformation representing the strongest interaction between the ligand and the protein. This approach has significantly contributed to the molecular understanding of ligand binding behavior on the target protein.

Results and discussion

In this study, 3-alkyl(aryl)-4-(3-methoxy-4-hydroxybenzylideneamino)-4,5-dihydro-1*H*-1,2,4-triazol-5-one **3**(**a**-**g**) Schiff bases have been synthesized from the reaction with 3-methoxy-4-hydroxybenzaldehyde (**2**) of 3-alkyl(aryl)-4-amino-4,5-dihydro-1*H*-1,2,4-triazol-5-one (**1**) compounds [55]. Seven new 1-(2,6-dimethylmorpholin-4-yl-methyl)-3-alkyl(aryl)-4-(3-methoxy-4-hydroxybenzylideneamino)-4,5-dihydro-1*H*-1,2,4-triazole-5-one compounds **4**(**a**-**g**) have been synthesized by reacting with 2,6-dimethylmorpholine in the presence of formaldehyde according to the Mannich reaction of synthesized these Schiff bases (Scheme 1).

Spectral study results

In this study, the structures of seven newly synthesized Mannich base derivatives were confirmed by detailed interpretation of their IR and NMR spectra. The IR spectra exhibited a characteristic band between 1584 and 1593 cm^{-1}, attributed to the azomethine (νC = N) stretching vibration, which supports the successful formation of the Schiff base bond. This band is consistent with the literature for azomethine-containing compounds,



Scheme 1 Synthesis pathway of 1–4 (**a**-**g**) compounds

where the ν(C = N) vibration typically appears around 1580–1610 cm^{-1}, depending on the electronic environment and conjugation [56]. Another prominent absorption band was observed between 1692 and 1704 cm^{-1}, corresponding to the carbonyl (νC = O) group, suggesting the presence of a ketone, amide, or ester group. These wavenumbers lie in the typical range for conjugated carbonyl groups and are slightly shifted due to potential intramolecular hydrogen bonding or resonance effects [57]. Additionally, broad absorption bands in the 3023–3500 cm^{-1} region, characteristic of O–H stretching vibrations in phenolic compounds, were observed. The width of these bands suggests the possibility of intramolecular hydrogen bonding, particularly involving the hydroxyl group in the 3-methoxy-4-hydroxybenzylideneamino moiety. Such broad O–H stretching is common in aromatic systems with ortho-hydroxy substituents and has been frequently reported in related compounds [58]. 1 H-NMR spectra further supported the structural features observed in the IR analysis. A singlet appearing in the 9.43–9.49 ppm range was attributed to the azomethine proton (–CH = N), which is usually deshielded due to the electron-withdrawing nature of the imine nitrogen and its conjugation with the aromatic ring. This chemical shift is consistent with previous findings in Schiff base derivatives, where the azomethine proton appears in the 8.5–9.8 ppm range [59]. The methylene protons of the Mannich group (NCH_2N) have been identified as singlets or multiplets in the range 4.51–4.69 ppm, depending on the surrounding environment. These chemical shifts are consistent with literature values for Mannich-type methylene bonds adjacent to nitrogen atoms, which are generally found between 4.3 and 4.8 ppm [60]. A singlet in the 3.81–3.86 ppm range was attributed to the methoxy group protons ($–OCH_3$) attached to the aromatic ring. The narrow range and singlet pattern indicate a consistent substitution pattern in all synthesized derivatives. This region is typical for aryl-OCH_3 protons and supports the presence of a 3-methoxy-4-hydroxyphenyl motif [61]. The ^{13}C-NMR spectra showed diagnostic chemical shifts supporting proton assignments. The imine carbon (–C = N) appeared in the range of 154.82–158.18 ppm, consistent with chemical shifts reported for imine carbons conjugated with aromatic systems. The methylene carbon of the Mannich base moiety, NCH_2N, was observed in the range of 55.52–56.05 ppm, consistent with literature reports for such systems. Furthermore, the methoxy carbon was observed in the range of 55.57–56.05 ppm, typical of OCH_3 groups in aromatic rings. Although the close shifts of the methylene and methoxy

Table 1 The compounds' reducing power

Compounds	Reducing Power		
	100	250	500
4a	0.115	0.144	0.145
4b	0.136	0.149	0.149
4c	0.120	0.128	0.139
4d	0.117	0.135	0.138
4e	0.117	0.135	0.138
4f	0.062	0.063	0.079
4 g	0.104	0.115	0.129
BHA	0.882	1.184	1.272
BHT	0.380	0.462	0.723
α-Tocopherol	0.534	0.934	1.175
Absorbance of control reaction: **0.140**			

carbons reflect similar hybridization and electron-donating environments, their different chemical environments are clearly evident in the spectra [62]. Taken together, the IR and NMR spectral data confirm the successful synthesis and expected structure of the Mannich base derivatives, with each functional group clearly supported by characteristic spectral signatures consistent with those reported in recent literature.

Reducing power

At various concentrations, the compounds' reducing powers were examined, and the outcomes were contrasted with those of BHT, BHA and α-tocopherol. The measured absorbance data have been given in Table 1. The findings obtained from the synthesized compounds' reducing power tests showed that the compounds did not have reducing properties and increased depending on the concentration. However, we observed that some compounds had higher reducing power than others. The compounds' reducing power graph utilizing the values given in Table 1 has been given in Fig. 1. When we examine Fig. 1, the synthesized compounds' absorbance values are lower than the standards. The order of reducing power of compounds and standards is as follows: BHA > α-tocopherol > BHT > 4b > 4a > 4d > 4c > 4 g. There is a direct proportion between the increase in the reducing power of the sample and the absorbance of the reaction solution. Similar results were obtained in the reducing power study conducted by Gürsoy-Kol et al. [44]. In this study, all the amounts of compounds showed lower absorbance than standard antioxidants. Thus, no activity was observed to reduce metal ion complexes to lower oxidation states or participate in any electron transfer reactions.

Free radical scavenging activity

To determine the DPPH radical scavenging activity in the reaction medium, the following formula was applied. Here, A_0 is the control reaction absorbance, whereas A_1 is the absorbance of the sample or standard. Absorbance values obtained at 517 nm using UV spectrophotometry and the corresponding % free radical scavenging activities have been given in Table 2. The data obtained as a result of the new synthesized compound's radical scavenging activity tests and the reference antioxidant substances utilized (BHA, α-tocopherol, and BHT) have been displayed in the graph below (Fig. 2). In the graph,

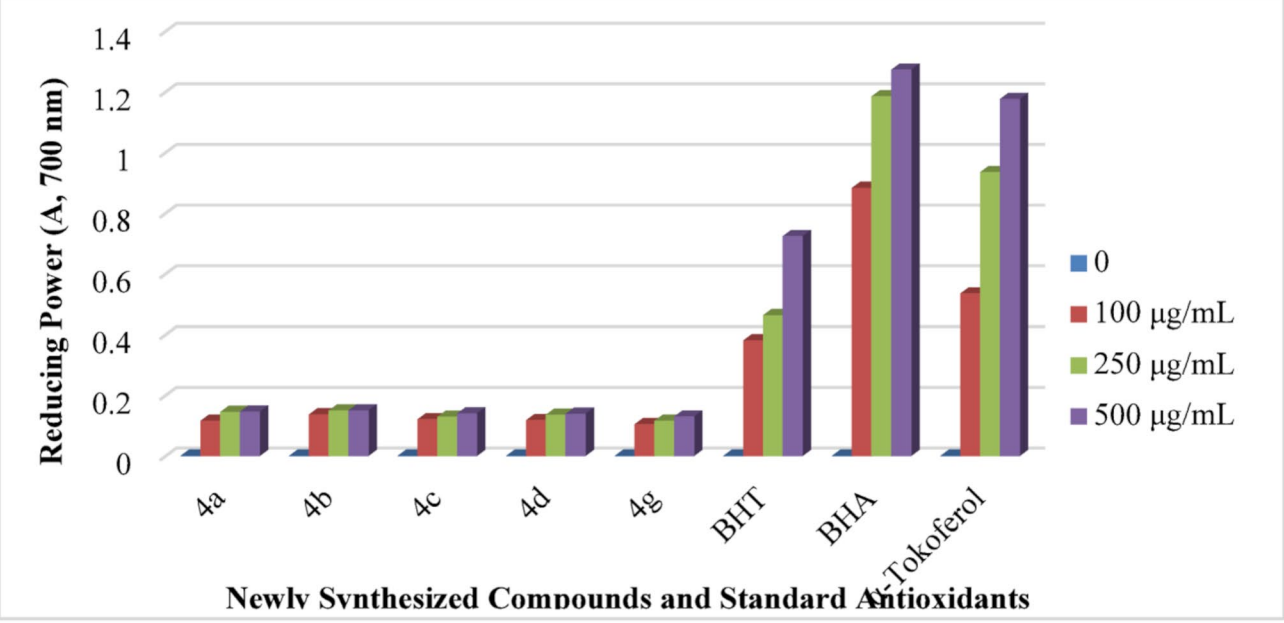


Fig. 1 Reducing power of **4a**, **4b**, **4c**, **4d** and **4 g** compounds and standard antioxidants

Table 2 Measured absorbence values of synthesized compounds' free radical scavenging activities

Compounds	Absorbance and %free radical scavenging activity					
	12.5		25		37.5	
	A	% Activity	A	% Activity	A	% Activity
4a	0.103	23.7	0.090	33.3	0.075	44.4
4b	0.106	21.5	0.090	33.3	0.077	43.0
4c	0.110	18.5	0.091	32.6	0.082	39.3
4d	0.097	28.1	0.086	36.3	0.069	48.9
4e	0.107	20.7	0.098	27.4	0.086	36.3
4f	0.127	5.9	0.093	31.1	0.082	39.3
4 g	0.107	20.7	0.097	28.1	0.085	37.0
BHA	0.035	85.0	0.035	87.9	0.048	89.3
BHT	0.073	45.7	0.051	63.6	0.051	77.1
α-Tocopherol	0.018	89.3	0.018	89.3	0.017	90.0

Absorbance of control reaction: **0.135**

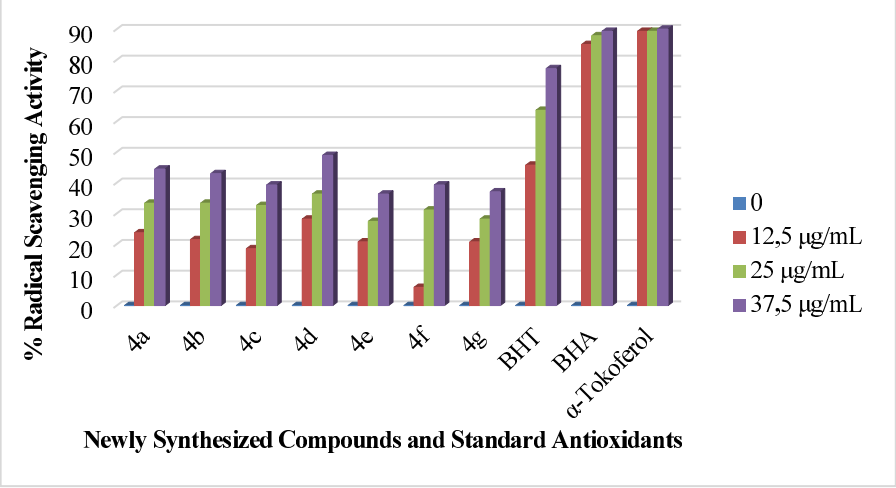


Fig. 2 Free radical scavenging activities and standard antioxidants of synthesized compounds

the free radical scavenging activities of some newly synthesized molecules, measured at different concentrations at 517 nm, have been given as % inhibition. In line with the obtained data, depending on the concentration, we found that the newly produced compounds' activity increased. When we examined the graph in Fig. 2, comparing the synthesized compounds to the standards, we found that their free radical scavenging activity was poor. The reduced absorbance of the reaction mixture is directly proportional to the sample's capacity to scavenge free radicals. Similar results were obtained in the free radical scavenging activity study conducted by Haydar Yüksek et al. [63]. Bu çalışmada, The newly synthesized compounds did not show significant activity as radical scavengers, but some compounds were reported to show higher activities than other compounds.

$$\%\ \text{Free radical scavenging activity} = \frac{A_0 - A_1}{A_0} \text{x} 100 \quad (1)$$

Metal chelate activity

The sample's metal chelating activity is directly correlated with the reaction mixture's drop in absorbance. Absorbance and % metal chelate activity values of **4**(**a**-**g**) compounds have been given in Table 3. In the graph in Fig. 3, the % inhibition of the synthesized compounds and the reference antioxidants EDTA and α-tocopherol activation have been shown. Generally, it has been reported that molecules including two or more functional groups like –SH, -COOH, –OH, C = O, $-PO_3H_2$, $-NR_2$, -O-, -S- in their structure with a suitable structure-function configuration will have chelation activity [50, 64]. In this study, we observed that the synthesized compounds have high metal chelation activity because of the presence of –OH, C = O, $-NR_2$, -O- groups. When we examined the graph in Fig. 3, we observed that the synthesized compound's chelating activities were higher than EDTA, while α-tocopherol, one of the reference substances, had lower activity. Similar results were obtained in the metal chelate activity study conducted by Gürsoy-Kol et al. In

Table 3 Measured absorbence values of synthesized compounds' metal chelate activities

Compounds	Absorbance and % metal chelate activity					
	30		45		60	
	A	% Activity	A	% Activity	A	% Activity
4a	0.043	76.5	0.042	77.0	0.042	77.0
4b	0.044	76.0	0.042	77.0	0.042	77.0
4c	0.043	76.5	0.041	77.6	0.042	77.0
4d	0.041	77.6	0.041	77.6	0.041	77.6
4e	0.042	77.0	0.042	77.0	0.043	76.5
4f	0.041	77.6	0.041	77.6	0.040	78.1
4 g	0.045	75.4	0.043	76.5	0.040	78.1
EDTA	0.032	58.5	0.031	59.0	0.030	60.7
α-Tocopherol	0.076	82.5	0.075	83.1	0.072	83.6

Absorbance of control reaction: **0.183**

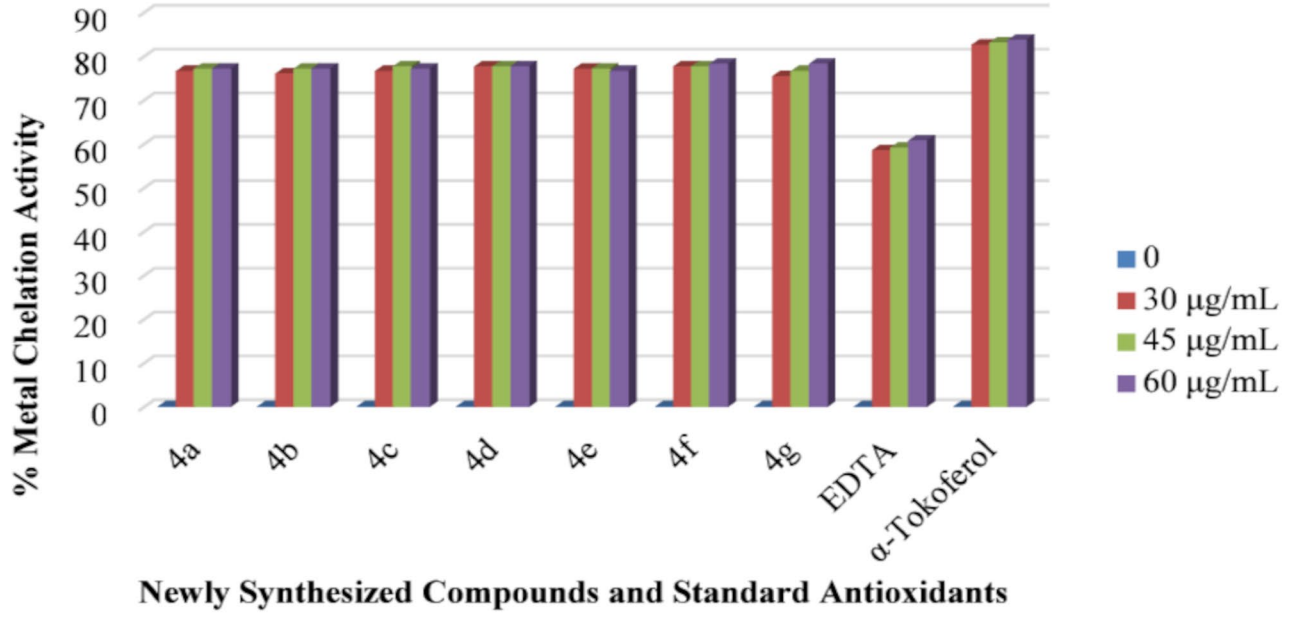


Fig. 3 Metal chelate activities and standard antioxidants of synthesized compounds

this study, newly synthesized compounds were analyzed for their in-vitro potential antioxidant capacity in three different experiments. All compounds were reported to show significant activity for the metal chelating effect [65]. Using the following formula, the percentage suppression of ferrozine-Fe^{+2} complex production was calculated:

$$\text{Chelate Percentage} = \frac{A_0 - A_1}{A_0} x100 \qquad (2)$$

Antimicrobial activity results

The antimicrobial properties of the synthesized compound were tested against 6 different bacteria using the agar well method. The results have been given in Table 4. *Neomycin* (3385), *ampicillin* (3261), and *streptomycin* (3385) were used as standard chemicals. In Figs. 4, 5 and 6, images showing the antimicrobial activity effects of the synthesized compounds against 6 different bacteria have been given. Antimicrobial activity results of the synthesized molecules have been given in Table 5. When we examined the data in Table 5, the synthesized compounds showed the best activity against *Bacillus cereus* bacteria, while they showed the weakest activity against *Bacillus subtilis* bacteria. Among the synthesized compounds, compound **4e** showed the best activity against 6 different bacteria. We observed that the antimicrobial activity of the seven new Mannich bases **4**(**a**-**g**) synthesized, which include 1,2,4-triazole and 2,6-dimethylmorpholine, varied depending on the type of substituent such as (R = a – g). In a study conducted by Kol, O.G and et al., 7 new 2-[1-(morpholine-4-yl-methyl)-3-alkyl/aryl-4,5-dihydro-1*H*-1,2,4-triazol-5-on-4-yl-azomethine)-

Table 4 The synthesized compounds' ZONE diameter values against bacteria

Compound Code	Bacillius Subtilis	Bacillus Cereus	Pseudomonas aeruginosa	Klebsiella pneumoniae	Staphlacocus aureus	Esherichia Coli
4a	10	28	9	14	14	10
4b	12	16	8	9	8	9
4c	-	19	9	9	13	-
4d	-	14	-	8	10	-
4e	12	21	-	19	8	10
4f	-	20	-	11	8	8
4 g	-	16	8	9	11	-
Streptomycin	33	36	36	35	37	34
Neomycin	17	17	17	16	13	16
Ampicillin	33	36	36	35	37	34

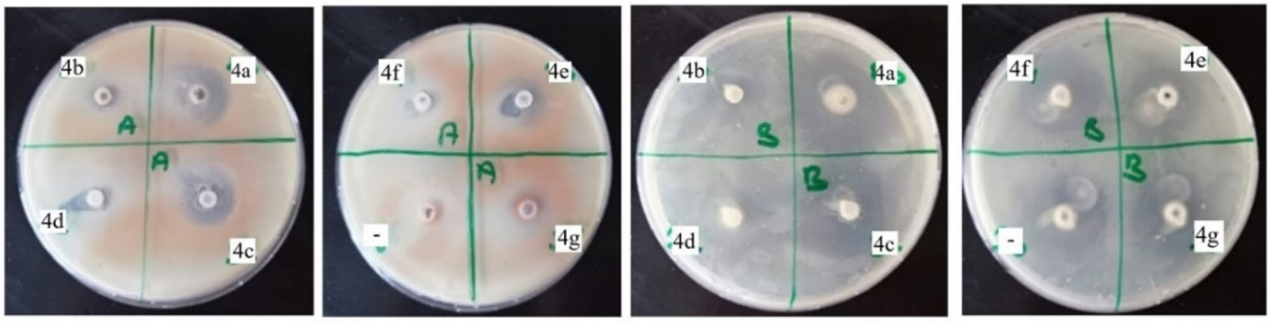


Fig. 4 Picture showing of synthesized compounds' antimicrobial effects against *Bacillus substilis* and *Bacillus Cereus*

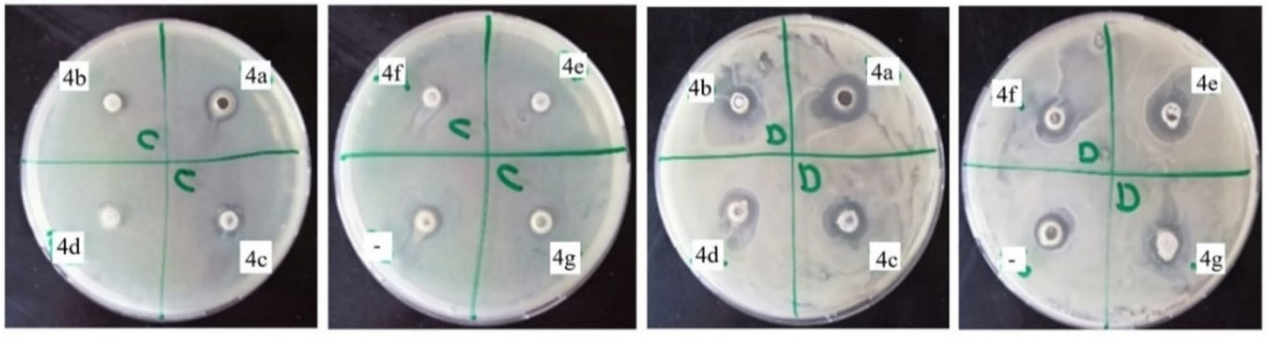


Fig. 5 Picture showing of synthesized compounds' antimicrobial effects against *Pseudomonas aeruginosa* and *Klebsiella pneumoniae*

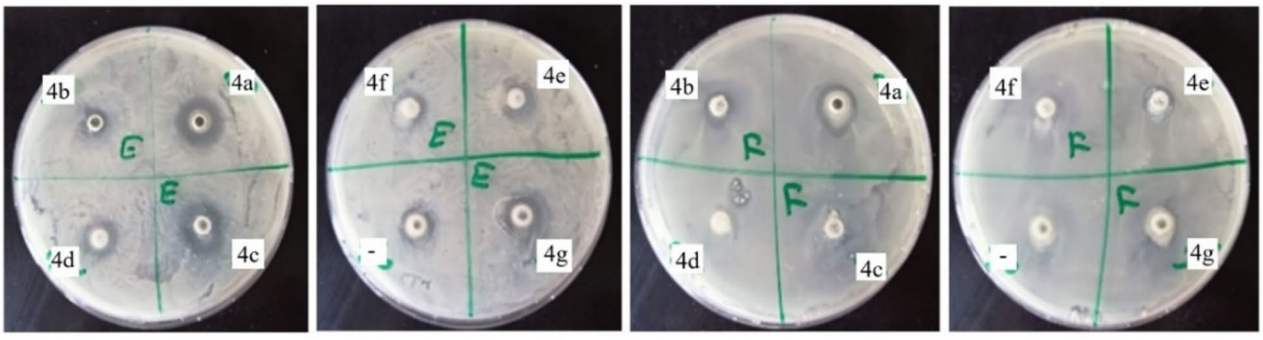


Fig. 6 Picture showing of synthesized compounds' antimicrobial effects against *Staphlacocus aureus* and *Esherichia Coli*

Table 5 The synthesized compounds' antimicrobial activity results

	ZONE diameter values (mm)					
Compounds	**Bacillius Subtilis**	**Bacillus Cereus**	**Pseudomonas aeruginosa**	**Klebsiella pneumoniae**	**Staphlacocus aureus**	**Esherichia Coli**
4a	+	+++	+	++	++	+
4b	++	++	+	+	+	+
4c	-	+++	+	+	++	-
4d	-	++	-	+	+	-
4e	++	+++	-	+++	+	+
4f	-	+++	-	++	+	+
4 g	-	++	+	+	++	-
Streptomycin	+++	+++	+++	+++	+++	+++
Neomycin	+++	+++	+++	++	++	++
Ampicillin	+++	+++	+++	+++	+++	+++

Table 6 The physico-chemical properties of the synthesized compounds

Code	Lipophilicity consensus log *P*	Physico-chemical properties									
		MW[a] g/mol	Heavy Atoms	Aromatic heavy atoms	Rot. bond	H acceptor bond	H donor bond	MR[b]	TPSA[c] (A^2)	% ABS[d]	Colour
4a	1.50	375.42	27	11	5	7	1	105.29	94.11	76.53	White
4b	2.73	403.48	29	11	7	7	1	114.90	94.11	76.53	White
4c	2.75	451.52	33	17	7	7	1	129.77	94.11	76.53	White
4d	2.95	465.54	34	17	7	7	1	134.74	94.11	76.53	White
4e	2.80	481.54	35	17	8	8	1	136.27	103.34	73.34	White
4f	3.15	485.96	34	17	7	7	1	134.78	94.11	76.53	White
4 g	2.66	437.49	32	17	6	7	1	125.76	94.11	76.533+	White

[a]MW, molecular weight; [c]TPSA, topological polar surface area; [b]MR, molar refractivity; [d]ABS%: absorption percent

phenyl-benzenesulfonates compounds were obtained by reactions with formaldehyde and morpholine. Antimicrobial activity of the synthesized compounds against six bacteria was determined using the agar well diffusion method [66]. In a study conducted by Özdemir, G. et al., six new 1-(2,6-dimetilmorfolin-4-il-metil)-3-alkil(aril)-4-[3-etoksi-(4-benzensülfoniloksi)-benzilidenamino]-4,5-dihidro-1*H*-1,2,4-triazol-5-on compounds were synthesized. Antimicrobial activity of the synthesized compounds against six bacteria was determined using the agar well diffusion method [67]. In a study conducted by Yilmaz, Y. et al., six new 4-[1-(2,6-dimethylmorpholin-4-yl-methyl)-3-alkyl(aryl)-4,5-dihydro-triazol-5-on-4-yl-azomethine]-2-methoxyphenyl benzoates compounds were synthesized. The synthesized compounds were examined for in-vitro antimicrobial properties against 6 different microorganisms [68]. These studies scanned in the literature prove that the antimicrobial activity of 1,2,4-triazole derivatives varies depending on the type of substituent such as (R = a – g).

Biochemical results

ADME analysis

ADME (Absorption, Distribution, Metabolism, and Elimination) analyses provide fundamental information about the pharmacokinetic properties and biological aspects of a population. A potent substance must be adequately distributed, metabolized slowly, and eliminated harmlessly. If ADME degradation is poor, these results are likely to be inaccurate [69]. Lipinski's Rule of Five is widely used to assess drug-like properties and determine whether a candidate compound is drug-like. According to these rules, a compound should have: fewer than 5 hydrogen bond donors, fewer than 10 hydrogen bond acceptors, a lipophilicity coefficient (LogP) of less than 5, a molar refractive index between 40 and 130, and a molecular weight of less than 500 daltons. Compounds that meet at least two of these rules demonstrate high drug-likeness, while compounds that meet fewer than two rules demonstrate lower drug-likeness [70]. The synthesized compound's physicochemical and lipophilic properties have been given in Table 6. Of the synthesized compounds, compounds **4a**, **4b**, **4c**, and **4 g** were found to fulfill all five of Lipinski's rules. Compounds **4d**, **4e**, and **4f** violated only one rule, the molar refractive index (40–130). Despite this, these compounds demonstrate high drug similarity because they fulfill at least four of the five rules and are suitable for evaluation as drug candidates. Compounds with positive LogP values are lipophilic, while compounds with negative LogP values are hydrophilic [71]. The compounds in the study had LogP values between 1.50 and 3.15, indicating that they are lipophilic.

Lipophilic structures can easily pass through cell membranes and dissolve in oil, increasing bioavailability. In addition to Lipinski's rules, a drug's topological polar surface area (TPSA) is also an important pharmacokinetic determinant. Compounds with TPSA values below 140 Å² generally have good oral bioavailability [72]. The TPSA values of the compounds synthesized in this study were measured between 94.11 and 103.34 Å², suggesting that these compounds may be good drug candidates. Percent oral absorption was calculated using the formula A% = 109 - (0.345 × TPSA); the compounds were found to have absorption rates of 76.53% and 73.34%, respectively. The structure, color regions, and physicochemical parameters presented in Fig. 7 support these assessments. Similarly, the pink regions in the polar surface area maps in Fig. 7 indicate that the compounds have favorable properties for oral bioavailability. The radar diagrams show that the compounds do not deviate from the saturation region but remain within the pink area, which is considered a positive indicator for oral bioavailability.

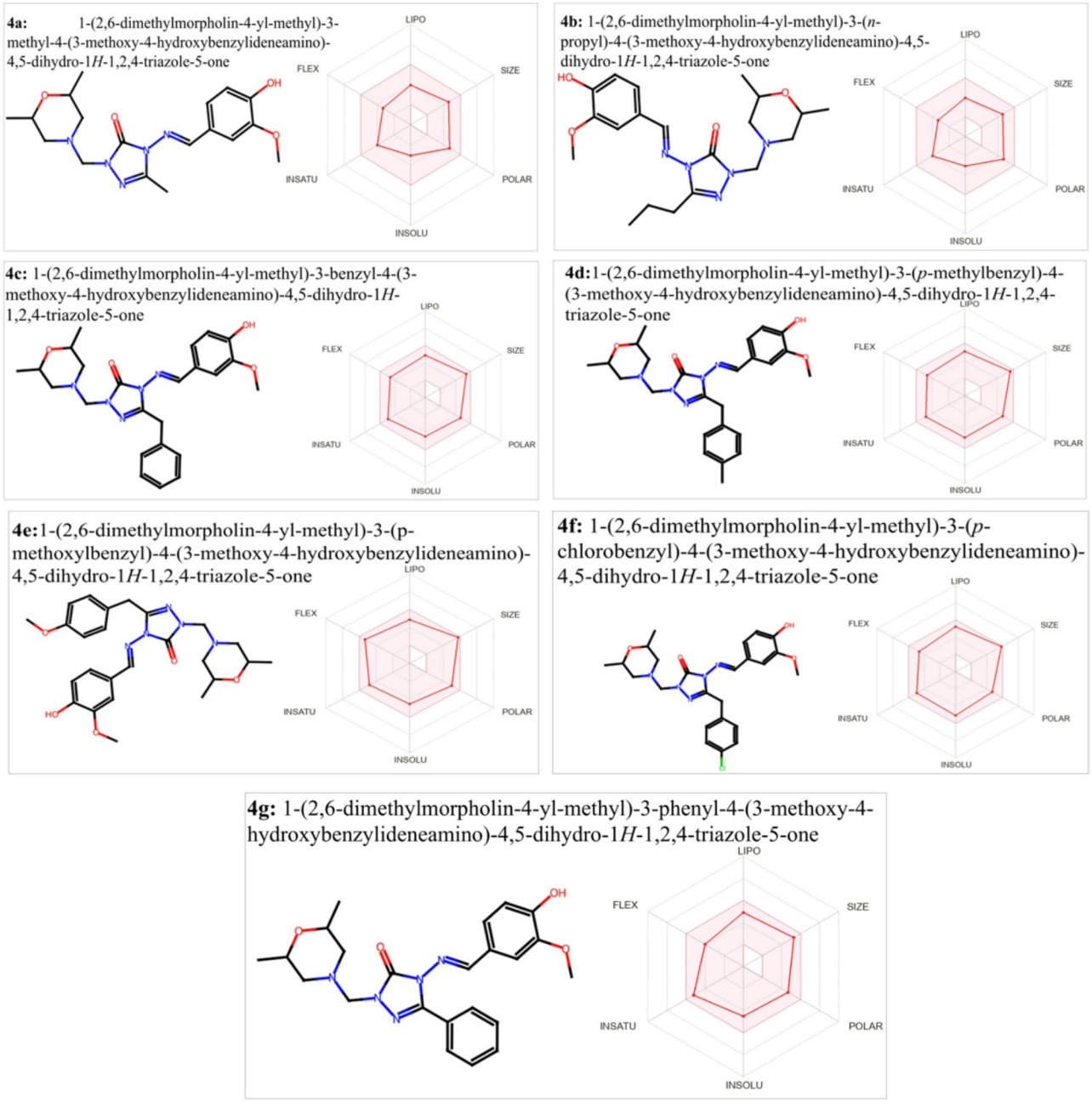


Fig. 7 Structure, color regions and physicochemical parameters of synthesized compounds

Molecular docking analysis

Molecular docking is a key method in structure-based drug design, accelerating and simplifying the discovery process of new drug candidates. This method allows for digital screening of ligand-protein interactions by predicting the binding conformations and affinities of ligands to target proteins [73]. In this study, in silico molecular docking analyses were performed using the Schrödinger Maestro Molecular Modeling Platform [35] to investigate the possible interactions of the synthesized compounds with Glutathione S-transferase (GST) and Butyrylcholinesterase (BChE) enzymes. Crystal structures of GST (PDB ID: 5J41) and BChE (PDB ID: 6SAM) enzymes were downloaded from the Protein Data Bank for use in docking analyses [54]. These two enzymes are widely reported in the literature to be used as biological targets associated with Alzheimer's disease [72]. It is reported in the literature that these two enzymes are widely used as biological targets associated with Alzheimer's disease [74]. Molecular docking results have been presented in Table 7. Analysis of the data revealed that compounds coded **4d**, **4e**, and **4f** exhibited the strongest binding scores against the BChE and GST enzymes, respectively. Specifically, compound 4d showed the highest binding score of -9.91 kcal/mol with the BChE enzyme, while compound 4f achieved the best docking score of -8.37 kcal/mol with the GST enzyme. Additionally, ADME (Absorption, Distribution, Metabolism, and Excretion) analysis results support the molecular docking findings. These analyses revealed that compounds **4d** and **4e** possessed the most favorable pharmacokinetic profiles. In light of these findings, compounds **4d** and **4e**, which exhibit high binding affinities and favorable ADME properties, are considered potential structure-based drug candidates for the treatment of Alzheimer's disease.

In Figs. 8, 2D and 3D images obtained as a result of the interaction of the synthesized **4d** compound with the BChE enzyme have been given. The docking score obtained in the interaction of compound **4d** with the BChE enzyme was found to be -9.91 cal/mol. In **4d** compound, were observed conventional hydrogen bonds of ASN-289 (5.04 Å), THR-120 (4.30 Å), and unfavorable donor-donor bonds of ASN-68 (4.48 Å) at the oxygen of the hydroxybenzyldene group, methoxide, and the oxygen of the triazole. We observed TRP-82 (5,07 Å), TRP-430 (4,40 Å), ALA-328 (3,96 Å), TYR-332 (4,58 Å), PHE-398 (5,84 Å) and LEU-286 (5,21 Å) Pi-alkyl bonds in the methyl groups of 2,6-Dimethylmorpholine and *p*-methylbenzyline. While TRP-231 (3.58 Å) Pi-Pi T-shaped bonds were observed in the *p*-methylbenzyline ring of **4d** compound, were observed GLY-116 (4.96 Å) Amide-Pistacked bonds in the triazole ring. Additionally, in **4d** compound were observed HIS-438, ASP-70, GLY-78 and MET-437 the van der Waals bonds.

Table 7 Docking scores with GST, and BChE enzymes of synthesized compounds

Compounds	Docking Score (kcal/mol)	
	BChE (PDB: 6SAM)	GST (PDB: 5J41)
4a	-5.40	-5.56
4b	-5.70	-6.21
4c	-6.59	-6.49
4d	-9.91	-5.91
4e	-8.20	-8.37
4f	-6.80	-5.91
4 g	6.65	-6.71

In Figs. 9, 2D and 3D images obtained as a result of the interaction of the synthesized **4e** compound with the GST enzyme have been given. The docking score obtained in the interaction of compound **4e** with GST enzyme was found to be -8.37 cal/mol. In the **4e** compound, were observed conventional hydrogen bonding at SER-198 (4.91 Å), ALA-277 (3.89 Å) the oxygen of the hydroxybenzylidene group and the methoxy group, respectively. While **4e** compound, PHE-329 (4.69 Å), TYR-332 (6.11 Å) Pi-Pi T-shaped bonds were observed in the *p*-methoxybenzyl ring and triazole ring, respectively, were observed GLY-283 (5.65 Å) Amide-Pistacked bond in the 3-methoxy-4-hydroxybenzylideneamino ring. PHE-329 (4,69 Å), PHE-398 (6,06 Å), HIS-438 (4,83 Å), ALA-328 (5,08 Å), TRP-82 (5,34 Å) in the methyl groups of 2,6-dimethylmorpholine and PHE-329 (4,69 Å), PHE-398 (6,06 Å), HIS-438 (4,83 Å), ALA-328 (5,08 Å), TRP-82 (5,34 Å) in the methyl group of *p*-methoxybenzyl in the **4e** compound were observed Pi-alkyl bonds. Additionally, in the **4e** compound were observed GLY-116, VAL-288, SER-79 and THR-284 the van der Waals bonds.

SAR analysis

Significant intramolecular charge transfer from the electron donor component to the electron acceptor component via a conjugated channel is indicated by a small energy gap (ΔE). The smallness of the energy gap value depends on the HOMO-LUMO energy difference. The smaller this difference, the more chemically reactive and less stable the molecule is [75]. The calculated HOMO-LUMO energy gap values and images of frontier molecular orbitals of the synthesized compounds have been given in Fig. 10. The target compounds' **4**(**a**-**g**) calculated HOMO-LUMO energy gaps in this study are 4.30, 4.32, 4.08, 4.10, 4.05, 4.15, 4.11 eV, respectively. The lowest energy difference value among the newly synthesized molecules was found to be 4.05 for compound **4e**. By calculating LUMO, molecular weight, total energy, and volume, the relationship between antimicrobial activities and molecular properties was investigated to discover the structure-activity relationships (SAR) of new compounds. The antimicrobial activity is explained by the

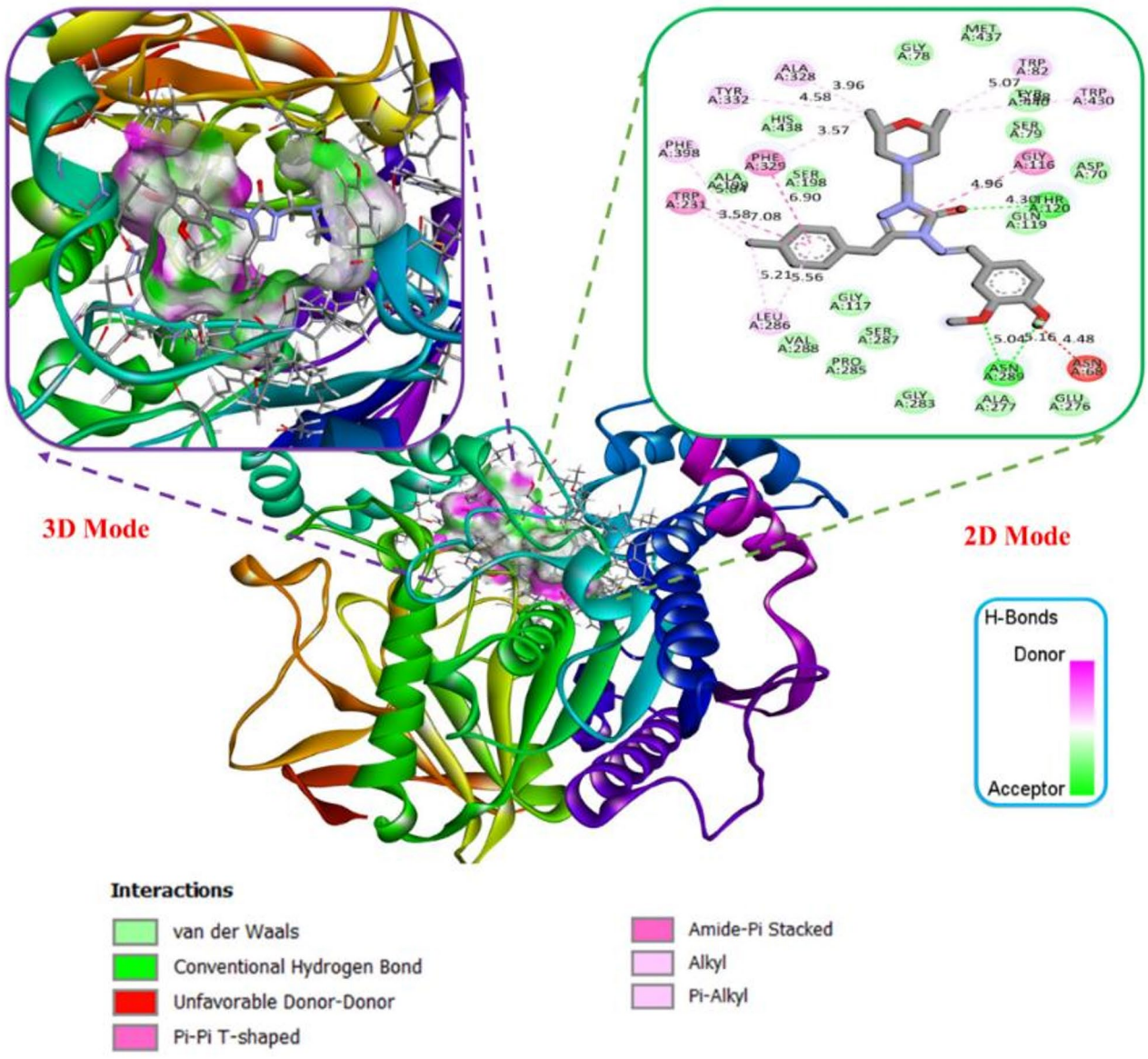


Fig. 8 Interacts with BChE (Docking Score:-9.91) enzym of synthesized compound **4d**; 3D view of the donor/acceptor surface of hydrogen bonds on the receptor, 2D view of ligand-enzyme interactions

density and LUMO. The LUMO value is a critical component in determining a molecule's electrophilicity and reactivity. Molecules with low lying LUMOs are more active than those with high lying LUMOs because they have a larger capacity to receive electrons. Compound **4e** has the lowest theoretical LUMO value (-1.706 eV), according to calculations of LUMO values. In the antibacterial research of a drug, the bacterial layer seems to join with the lipophilic layer because of the high reactivity and electrophilicity detected in the low-energy empty molecular orbital (LUMO). As a result, the bacterial membrane becomes more permeable, halting the organism's continued development. As a result, we may say that the composition and structure of molecules affect their antibacterial properties. A molecule's density shows how densely its atoms are packed. Mass and volume were computed theoretically and displayed in Table 8. We use the ratio of molecular weight to molecular volume to determine density. Density has an inverse relationship with reactivity and, hence, activity. At the lowest density, the molecule exhibits the most reactivity. All of these computations led to the conclusion that compound **4e** is the molecule with the highest antibacterial activity and the lowest density [76].

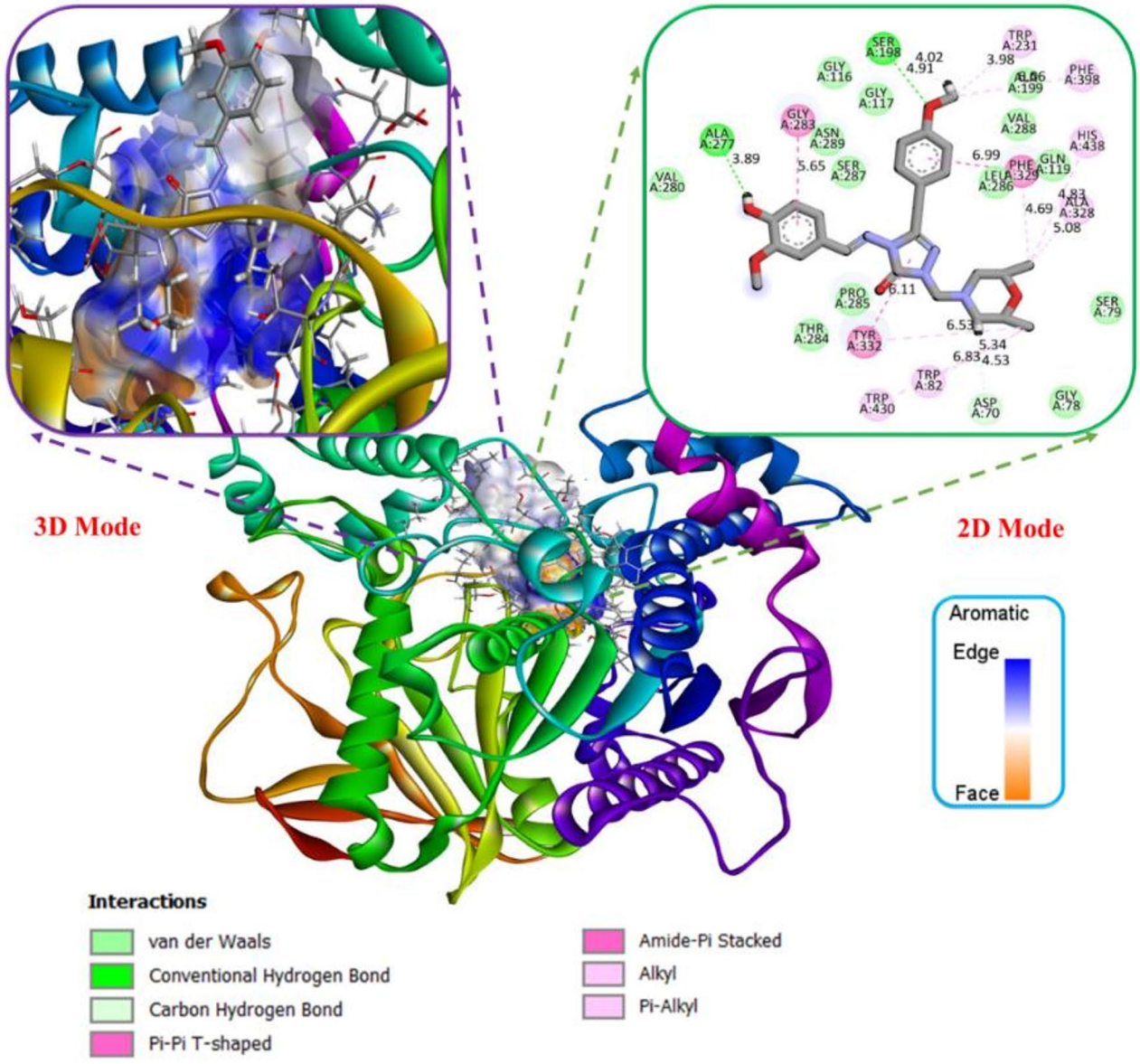


Fig. 9 Interacts with GST (Docking Score:-8.37) enzym of synthesized compound **4e**; 3D view of the donor/acceptor surface of aromatic bonds on the receptor, 2D view of ligand-enzyme interactions

Conclusion

In this study, seven new Mannich base derivatives (**4a**–**4 g**) were successfully synthesized, and their structural properties were characterized in detail using ^{1}H-NMR, ^{13}C-NMR, and IR spectroscopy. The biological potential of the compounds was evaluated under three main headings: antioxidant, antimicrobial, and molecular target interactions supported by theoretical (computational) analyses. In vitro analyses of antioxidant activity revealed that the synthesized compounds had very low free radical scavenging and reduction capacities. However, the high metal chelation activity of the compounds was attributed to the presence of functional groups such as –OH, C = O, $–NR_2$, and –O– in the structure. This result suggests that these compounds may exhibit potential protective effects against prooxidative metal ions. Antimicrobial tests were performed on six different bacterial strains, and the compounds generally exhibited moderate antibacterial activity. In particular, compound **4e** was determined to be the most potent antimicrobial agent in the series, exhibiting significant inhibitory activity against all tested bacteria. This effect is thought to be related to the synergistic effect of the electronic and structural properties of the molecule. In silico molecular docking analyses performed to understand the possible mechanisms of biological activity revealed the potential interaction of the synthesized

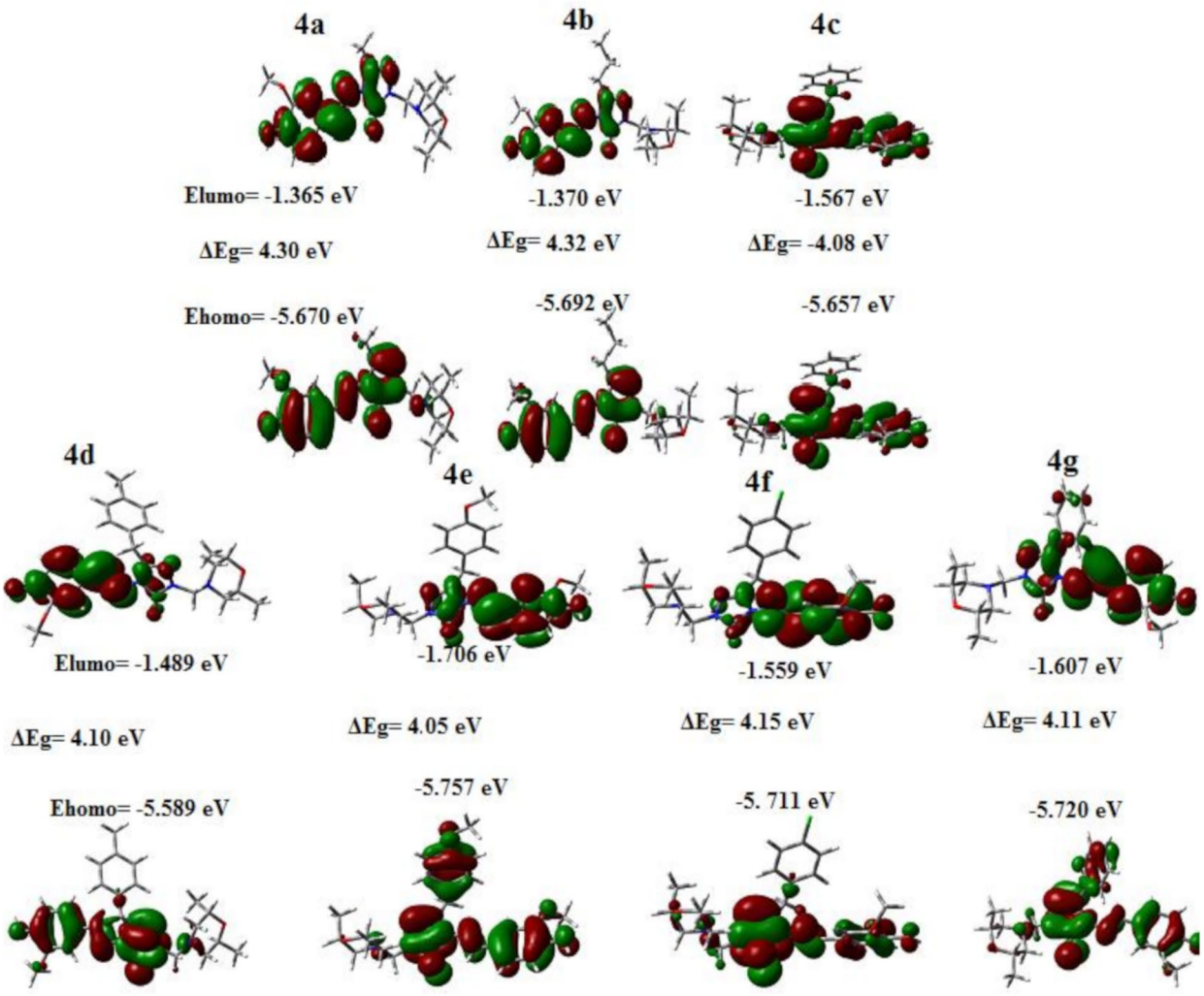


Fig. 10 Calculated HOMO-LUMO energy gaps values and frontier molecular orbitals of the synthesized compounds

Table 8 Some parameters of **4**(**a**-**g**) compounds calculated using the DFT method

Compounds	Total Energy (a.u)	LUMO (eV)	Mol. Wt. (amu)	Volume (Å^3)	Density
4a	-1275.60586552	-1.365	375.1906	235.002	1.3691
4b	-1354.23199528	-1.370	403.2219	287.766	1.4012
4c	-1659.296693	-1.567	451.2219	331.462	1.3613
4d	-1698.612351	-1.489	465.2376	342.557	1.3581
4e	-1773.830499	-1.706	481.2325	365.597	1.3162
4f	-2118.884017	-1.559	485.1829	332.587	1.4588
4 g	-1619.975061	-1.607	437.2063	298.563	1.4643

compounds with glutathione S-transferase (GST) and butyrylcholinesterase (BChE), target enzymes associated with Alzheimer's disease. As a result of these analyses, compound **4d** was determined to be the most potent inhibitor, achieving a binding score of -9.91 with BChE, while compound **4e** stood out with a binding score of -8.37 with GST. These results demonstrate not only antimicrobial but also neuroprotective potential of the compounds. In addition, the pharmacokinetic properties of the compounds were investigated using ADME (Absorption, Distribution, Metabolism, and Excretion) analyses, and all compounds were found to meet at least two of Lipinski's five rules. This indicates a good drug similarity profile for the synthesized structures. In this context, the obtained theoretical results strongly overlap with the experimental biological activities. Finally, structure–activity relationship (SAR) analyses were conducted using density functional theory (DFT). According to the

obtained DFT parameters, compound **4e** was found to have the lowest LUMO energy level, the lowest density value, and the narrowest HOMO–LUMO band gap (ΔE). These parameters indicate that the molecule has high reactivity and strong potential to interact with biological targets. These results are consistent with the strong antimicrobial activity of compound **4e** and its high binding score on the GST enzyme.

Author contributions

VT, KG, HY, GK designed and coordinated the study, VT, KG, HY, made analyzes. VT, KG, GK. – performed the literature review and drafted the manuscript. All authors have read and agreed to the published version of the manuscript.

Funding

The authors declare that they received no financial support.

Data availability

The datasets generated and analysed during the current the study are available from the corresponding author on reasonable request.

Declarations

Ethics and consent to participate

Not applicable.

Consent for publication

Not applicable.

Competing interests

The authors declare no competing interests.

Author details

[1]Nursing Department, Health Sciences Faculty, Şırnak University, Şırnak, Turkey
[2]Department of Chemistry, Faculty of Science and Letters, Kafkas University, Kars, Turkey
[3]Department of Chemistry and Chemical Processing Technologies, Vocational School, Kafkas University, Kars, Turkey

Received: 26 February 2025 / Accepted: 14 August 2025
Published online: 22 August 2025

References

1. Hassan SA, Ziwar JB, Aziz Dm, Abdullah MN. Sonochemical synthesis of new Thiazolidin-4-one derivatives as potent anticancer and antimicrobial agents with Docking design, and energy gap Estimation. J Mol Struct. 2024;1301:137282. https://doi.org/10.1016/j.molstruc.2023.137282.
2. Hassan SA, Abdullah MN, Aziz DM. An efficient One-pot three-component synthesis, molecular docking, ADME and DFT predictions of new series Thiazolidin-4-one derivatives bearing a sulfonamide moiety as potential antimicrobial and antioxidant agents. Egypt J Chem. 2022;65:133–46. https://doi.org/10.21608/ejchem.2022.104381.4819.
3. Abdullah MN, Osw P, Hassan SA, Othman S. Two new cyclohexenone derivatives: synthesis, DFT estimation, biological activities and molecular Docking study. J Mol Struct. 2024;1301:137361. https://doi.org/10.1016/j.molstruc.2023.137361.
4. Hassan SA, Aziz DM, Abdullah MN, Bhat AR, Dongre RS, Hadda TB, Almalki FA, Kawsar SMA, Rahiman AK, Ahmed S, Abdellattif MH, Berredjem M, Sheikh SA, Jamalis J. In vitro and in vivo evaluation of the antimicrobial, antioxidant, cytotoxic, hemolytic activities and in Silico POM/DFT/DNA-binding and Pharmacokinetic analyses of new sulfonamide bearing thiazolidin-4-ones. J Biomol Struct Dynamics. 2024;42:3747–63. https://doi.org/10.1080/07391102.2023.2226713.
5. Gao F, Wang T, Xiao J, Huang G. Antibacterial activity study of 1,2,4-triazole derivatives. Eur J Med Chem. 2019;173:274–81. https://doi.org/10.1016/j.ejmech.2019.04.043.
6. Yüksek H, Akyıldırım O, Yola ML, Gürsoy-Kol Ö, Çelebier M, Kart D. Synthesis, in vitro antimicrobial and antioxidant activities of some new 4,5-Dihydro-1H-1,2,4-triazol-5-one derivatives. Arch Pharm. 2013;346:470–80. https://doi.org/10.1002/ardp.201300048.
7. Rajesab P, Mathada BS, Niranjan V, Maurya A, Setlur AS, Prasad O, Chandrashekar K, Sinha L. Insights into novel Isoniazide encompassing triazolo[4,3-b][1,2,4]triazoles as Anti-TB, antioxidant and antidiabetic agents: A spectral analysis, DFT calculations, ADME, in vitro, and in Silico molecular modeling studies. J Mol Struct. 2025;1334:141876. https://doi.org/10.1016/j.molstruc.2025.141876.
8. Sridhar BT, Javeed M, Karunakar P, Nagesh GY, Ahmed M, Nalini R, Basavarajaiah SM. Investigating the molecular interactions of 11-substituted-1-(4-chlorophenyl)-8H-indolo[3,2-c][1,2,4]triazolo[3,4-a]isoquinolines for antimicrobial potential: synthesis, spectral, in vitro and in Silico study interpretations. J Mol Struct. 2024;1312:138617. https://doi.org/10.1016/j.molstruc.2024.138617.
9. Avci A, Taşci H, Kandemir Ü, Can ÖD, Gökhan-Kelekçi N, Tozkoparan B. Synthesis, characterization, and in vivo Pharmacological evaluation of novel Mannich bases derived from 1,2,4-triazole containing a Naproxen moiety. Bioorg Chem. 2020;100:103892. https://doi.org/10.1016/j.bioorg.2020.103892.
10. Gul HI, Tugrak M, Gul M, Mazlumoglu S, Sakagami H, Gulcin I, Supuran CT. New phenolic Mannich bases with piperazines and their bioactivities. Bioorg Chem. 2019;90:103057. https://doi.org/10.1016/j.bioorg.2019.103057.
11. Idhayadhulla A, Surendra Kumar R, Abdul Nasser AJ, Selvin J, Manilal A. Synthesis of some Mannich base derivatives and their antimicrobial activity study. Arab J Chem. 2014;7:994–9. https://doi.org/10.1016/j.arabjc.2010.12.025.
12. Bayrak H, Demirbas A, Karaoglu SA, Demirbas N. Synthesis of some new 1,2,4-triazoles, their Mannich and schiff bases and evaluation of their antimicrobial activities. Eur J Med Chem. 2009;44:1057–66. https://doi.org/10.1016/j.ejmech.2008.06.019.
13. Dorababu A, Kamble RR, Kamble AA, Kumbar MN, Shaikh SJ, Netalkar SP. Mannich bases of 1,2,4-Triazolones as potent Anti-Tubercular and antifungal agents. ChemistrySelect. 2019;4:2881–5. https://doi.org/10.1002/slct.201803933.
14. Hozien ZA, El-Mahdy AF, Markeb AA, Ali LS, El-Sherief HA. Synthesis of schiff and Mannich bases of new s-triazole derivatives and their potential applications for removal of heavy metals from aqueous solution and as antimicrobial agents. RSC Adv. 2020;10:20184–94. https://doi.org/10.1039/D0RA02872J.
15. Kotan G. Novel Mannich base derivatives: synthesis, characterization, antimicrobial and antioxidant activities. Lett Org Chem. 2021;18:830–41. https://doi.org/10.2174/1570178617999201216113719.
16. Pachuta-Stec A. Antioxidant activity of 1,2,4-Triazole and its derivatives: A Mini-Review. Mini-Rev Med Chem. 2022;22:1081–94. https://doi.org/10.2174/1389557521666210401091802.
17. Ceylan Ş, Cebeci YU, Demirbaş N, Batur ÖÖ, Özakpınar ÖB. Antimicrobial, antioxidant and antiproliferative activities of novel quinolones. ChemistrySelect. 2020;5:11340–6. https://doi.org/10.1002/slct.202002779.
18. Hamoud MMS, Osman NA, Rezq S, Abd El-wahab HAA, Hassan AEA, Abdel-Fattah HA, Romero DG, Ghanim AM. Design and synthesis of novel 1,3,4-Oxadiazole and 1,2,4-Triazole derivatives as Cyclooxygenase-2 inhibitors with Anti-inflammatory and antioxidant activity in LPS-stimulated RAW264.7 macrophages. Bioorg Chem. 2022;124:105808. https://doi.org/10.1016/j.bioorg.2022.105808.
19. Zalaru C, Dumitrascu F, Draghici C, Tarcomnicu I, Marinescu M, Nitulescu GM, Tatia R, Moldovan L, Popa M, Chifiriuc MC. New pyrazolo-benzimidazole Mannich bases with antimicrobial and antibiofilm activities. Antibiotics. 2022;11:1094. https://doi.org/10.3390/antibiotics11081094.
20. Lass-Flörl C. Triazole antifungal agents in invasive fungal infections: a comparative review. Drugs. 2011;71:2405–19.
21. Raic-Malic S, Mescic A. Recent trends in 1,2,3-Triazolo-Nucleosides as promising Anti-Infective and anticancer agents. Curr Med Chem. 2015;22:1462–99. https://doi.org/10.2174/0929867322666150227150127.
22. Ajmal M, Mahato AK, Khan M, Rawat S, Husain A, Almalki EB, Alzahrani MA, Haque A, Hakme MJM, Albalawi AS, Rashid M. Significance of Triazole in medicinal chemistry: advancement in drug design, reward and biological activity. Chem Biodivers. 2024;21:e202400637. https://doi.org/10.1002/cbdv.202400637.

23. Sirigineedi M, Srikanth M, Bellapukonda P. The Early Detection Of Alzheimer's Illness Using Machine Learning And Deep Learning Algorithms. J Pharm Negat. 2022;4852–9. https://doi.org/10.47750/pnr.2022.13.S09.603.
24. Zhang X, Song Q, Cao Z, Li Y, Tian C, Yang Z, Zhang H, Deng Y. Design, synthesis and evaluation of chalcone Mannich base derivatives as multifunctional agents for the potential treatment of alzheimer's disease. Bioorg Chem. 2019;87:395–408. https://doi.org/10.1016/j.bioorg.2019.03.043.
25. Boy S, Aras A, Türkan F, Akyıldırım O, Beytur M, Sedef Karaman H, Manap S, Yüksek H. Synthesis, spectroscopic analysis, and in vitro/in Silico biological studies of novel piperidine derivatives heterocyclic Schiff-Mannich base compounds. Chem Biodivers. 2021;18:e2100433. https://doi.org/10.1002/cbdv.202100433.
26. Tahiroğlu V, Uğur E, Coşkun E, Alayunt NÖ, Zorgör G. Protective role of BDNF in alzheimer's disease pathophysiology and its correlation with new biomarkers: can the role of BDNF be re-discussed? Adv Clin Exp Med. 2024;33:773–9. https://doi.org/10.3390/antibiotics11081094.
27. Ghotbi G, Mahdavi M, Najafi Z, Moghadam FH, Hamzeh-Mivehroud M, Davaran S, Dastmalchi S. Design, synthesis, biological evaluation, and Docking study of novel dual-acting thiazole-pyridiniums inhibiting acetylcholinesterase and β-amyloid aggregation for alzheimer's disease. Bioorg Chem. 2020;103:104186. https://doi.org/10.1016/j.bioorg.2020.104186.
28. Siddiqui SZ, Arfan M, Abbasi MA, Aziz ur R, Shah SAA, Parveen R, Ashraf M, Solangi M, Hussain S, Khan KM. Design, synthesis of triazole-based scaffolds, N-(substitutedphenyl)-2-(5-(4-methoxyphenyl)-4-phenyl-4H-1,2,4-triazol-3-ylthiol)acetamides: as potential anti-cholinesterase agents for neurodegenerative diseases. J Mol Struct. 2023;1289:135885. https://doi.org/10.1016/j.molstruc.2023.135885.
29. Patel A, Shah D, Patel Y, Patel S, Mehta M, Bambharoliya T. A review on recent development of novel heterocycles as acetylcholinesterase inhibitor for the treatment of alzheimers disease. Curr Drug Targets. 2023;24:225–46. https://doi.org/10.2174/1389450124666221213114500.
30. Roopa DL, Shyamsunder K, Karunakar P, Rajabathar JR, Venkatesulu A, Karnan M, Kiran KS, Selvaraj M, Basavarajaiah SM. Naphtho[2,1-b]furan derived triazole-pyrimidines as highly potential InhA and cytochrome c peroxidase inhibitors: synthesis, DFT calculations, drug-likeness profile, molecular Docking and dynamic studies. J Mol Struct. 2023;1287:135685. https://doi.org/10.1016/j.molstruc.2023.135685.
31. Basavarajaiah SM, Badiger J, Yernale NG, Gupta N, Karunakar P, Sridhar BT, Javeed M, Kiran KS, Rakesh B. Exploration of Indolo[3,2c]isoquinoline derived triazoles as potential antimicrobial and DNA cleavage agents: Synthesis, DFT calculations, and molecular modeling studies. Bioorganic Chemistry. 2023;137:106598. https://doi.org/10.1016/j.bioorg.2023.106598
32. Preat J, Loos P-F, Assfeld X, Jacquemin D, Perpète EA. DFT and TD-DFT investigation of IR and UV spectra of solvated molecules: comparison of two SCRF continuum models. Int J Quantum Chem. 2007;107:574–85. https://doi.org/10.1002/qua.21182.
33. Raman APS, Singh MB, Chaudhary M, Bahdur I, Jain P, Kaushik N, Choi EH, Kaushik NK, Lal AA, Singh P. DFT calculations, molecular Docking and SAR investigation for the formation of eutectic mixture using thiourea and Salicylic acid. J Mol Liq. 2022;362:119650. https://doi.org/10.1016/j.molliq.2022.119650.
34. Sarmah P, Deka RC. Anticancer activity of nucleoside analogues: A density functional theory based QSAR study. J Mol Model. 2010;16:411–8. https://doi.org/10.1007/s00894-009-0551-9.
35. Release S. 1: Maestro, Schrodinger, LLC, New York. 2019.
36. Studio BD. Dassault Systèmes Biovia Corporation. San Diego, USA. 2016.
37. SwissADME. 2024 [cited 2024 12.11.2024]; Available from: http://www.swissadme.ch/
38. Frisch GWTMJ, Schlegel HB, Scuseria GE, Robb MA, Cheeseman JR, Scalmani G, Barone V, Mennucci B, Petersson GA, Nakatsuji H, Caricato M, Li X, Hratchian HP, Izmaylov AF, Bloino J, Zheng G, Sonnenberg JL, Hada M, Ehara M, Toyota K, Fukuda R, Hasegawa J, Ishida M, Nakajima T, Honda Y, Kitao O, Nakai H, Vreven T, Montgomery JA Jr., Peralta JE, Ogliaro F, Bearpark M, Heyd JJ, Brothers E, Kudin KN, Staroverov VN, Kobayashi R, Normand J, Raghavachari K, Rendell A, Burant JC, Iyengar SS, Tomasi J, Cossi M, Rega N, Millam JM, Klene M, Knox JE, Cross JB, Bakken V, Adamo C, Jaramillo J, Gomperts R, Stratmann RE, Yazyev O, Austin AJ, Cammi R, Pomelli C, Ochterski JW, Martin RL, Morokuma K, Zakrzewski VG, Voth GA, Salvador P, Dannenberg JJ, Dapprich S, Daniels AD. Ö. Farkas, J.B. Foresman, J.V. Ortiz, J. Cioslowski, D.J. Fox, Gaussian 09. 2009.
39. Oyaizu M. Antioxidative activities of Browning reaction prepared from glucosamine. Jpn J Nutr. 1986;44:307–15.
40. Kotan G, Manap S, Yüksek H. Synthesis, characterization, antioxidant and DFT studies of some novel schiff base compounds. J Comput Biophys Chem. 2022;21:47–63. https://doi.org/10.1142/S2737416522500041.
41. Blois MS. Antioxidant determinations by the use of a stable free radical. Nature. 1958;181:1199–200.
42. Gören K, Kotan G, Manap S, Yüksek H. Synthesis, antimicrobial and antioxidant activities of 3-Alkyl(aryl)-4-(3-methoxy-4-hydroxybenzylideneamino)-4,5-dihydro-1H-1,2,4-triazol-5-one derivatives. Chem Afr. 2024;7:5273–89. https://doi.org/10.1007/s42250-024-01139-2.
43. Hamdi N, Mansour L, Al-Tamimi J, Al-Hazmy SM, Gurbuz N, Özdemir I. Synthesis and Investigation of Antimicrobial, Antioxidant, Enzymatic Inhibitory, and Antiproliferative Activities of Ruthenium (II) Complexes Bearing Benzimidazole-Based N-Heterocyclic Carbene (NHC) Ligands. PAHs. 2022;1–25 https://doi.org/10.1080/10406638.2022.2150659
44. Bahçeci Ş, Yıldırım N, Alkan M, Gürsoy-Kol Ö, Manap S, Beytur M, Yüksek H. Investigation of antioxidant, biological and acidic properties of new 3-alkyl (aryl)-4-(3-acetoxy-4-methoxybenzylidenamino)-4,5-dihydro-1H-1,2,4-triazol-5-ones. Pharm Chem J. 2017;4:91–101.
45. Kardaş F, Gürsoy-Kol Ö, Beytur M, Alkan M, Yüksek H. Synthesis and in vitro antimicrobial properties of some new 4-(2-Benzoxy-3-ethoxy)-benzylidenamino-4, 5-dihydro-1H-1, 2, 4-triazol-5-one derivatives. Int Res J Pure Appl Chem. 2017;15:1–9. https://doi.org/10.9734/IRJPAC/2017/37845.
46. Yüksek H, Kardaş F, Manap S, Alkan M, Albayrak Ö, Beytur M. Gürsoy-kol, synthesis and biological evaluation of new 2-Ethoxy-6-[4,5-dihydro-1H-1,2,4-triazol-5-one-4-yl iminomethyl]phenyl-4-nitro-benzoate derivatives. HJBC. 2017;45:153–61.
47. Gulcin İ, Alwasel SH. Metal ions, metal chelators and metal chelating assay as antioxidant method. Processes. 2022;10(132). https://doi.org/10.3390/pr10010132.
48. Wang T, Jónsdóttir R, Ólafsdóttir G. Total phenolic compounds, radical scavenging and metal chelation of extracts from Icelandic seaweeds. Food Chem. 2009;116:240–8. https://doi.org/10.1016/j.foodchem.2009.02.041.
49. Dinis TCP, Madeira VMC, Almeida LM. Action of phenolic derivatives (Acetaminophen, salicylate, and 5-Aminosalicylate) as inhibitors of membrane lipid peroxidation and as Peroxyl radical scavengers. Arch Biochem Biophys. 1994;315:161–9. https://doi.org/10.1006/abbi.1994.1485.
50. Türkyılmaz M, Tağı Ş, Özkan M. Effects of extraction solvents on polyphenol contents, antioxidant and antibacterial activities of pomegranate parts. Acad Food. 2017;15:109–18. https://doi.org/10.24323/akademik-gida.333632.
51. Hassan SA, Aziz DM, Abdullah MN, Bhat AR, Dongre RS, Ahmed S, Kalilur Rahiman A, Hadda TB, Berredjem M, Jamalis J. Design and synthesis of Oxazepine derivatives from sulfonamide schiff bases as antimicrobial and antioxidant agents with low cytotoxicity and hemolytic prospective. J Mol Struct. 2023;1292:136121. https://doi.org/10.1016/j.molstruc.2023.136121.
52. Hassan SA, Aziz DM, Kader DA, Ahmad HO, Noori M, Amin AAM, Qurbani HJ, Husein SM, Hamasdiq GH. Synthesis and characterization of Azo-Azomethine derivatives bearing thiazole moiety: in vitro antimicrobial, in vitro and in vivo anti-inflammatory, and cytotoxicity assessment, accompanied by computational molecular docking, RDG, ELF, DFT, and MEP analysis. J Mol Struct. 2024;1318:139294. https://doi.org/10.1016/j.molstruc.2024.139294.
53. Francl M, Pietro W, Hehre W, Binkley JS, Gordon MS, DeFrees DJ, Pople JA. J Chem Phys. 1982;77:3654.
54. Burley SK, Berman HM, Bhikadiya C, Bi C, Chen L, Di Costanzo L, Christie C, Dalenberg K, Duarte JM, Dutta S. RCSB protein data bank: biological macromolecular structures enabling research and education in fundamental biology, biomedicine, biotechnology and energy. Nucleic Acids Res. 2019;47:D464–74.
55. Ö, Gürsoy, Kol. Bazı 4, 5-dihidro-1H-1, 2, 4-triazol-5-on türevlerinin sentezi, yapılarının aydınlatılması, antioksidan ve asitlik özelliklerinin incelenmesi. Fen Bilimleri Enstitüsü, Doktora Tezi, 393s, Kars. 2008.
56. Muhammed Aziz D, Ali Hassan S. Synthesis, characterization, and evaluation of tetrazole derivatives with Pyrrole-2, 5-Dione moieties as urease inhibitors: exploring Structure-Activity relationships and computational insights. ChemistrySelect. 2024;9:e202401259. https://doi.org/10.1002/slct.202401259.
57. Hassan S, Abdullah M. Synthesis, spectroscopic study and biological activity of some new heterocyclic compounds derived from sulfadiazine. Iraqi J Sci. 2020;31:92–109. https://doi.org/10.21271/ZJPAS.31.6.10.
58. Aziz DM, Hassan SA, Amin AAM, Qurbani K, Aziz SB. A synergistic investigation of azo-thiazole derivatives incorporating thiazole moieties: a comprehensive exploration of their synthesis, characterization, computational insights, solvatochromism, and multimodal biological activity assessment. RSC Adv. 2023;13:34534–55. https://doi.org/10.1039/d3ra06469g.

59. Aziz DM, Hassan SA, Hamad OQ. Azo-azomethine complex activity and sensor potential toward Ca(II) ion in life samples: the spectroscopic and morphological studies. J Mol Struct. 2023;1293:136204. https://doi.org/10.1016/j.molstruc.2023.136204.
60. Bi LS, Anil B, Koca M, Demir Y, Gülçin İ. Novel Mannich bases with strong carbonic anhydrases and acetylcholinesterase Inhibition effects: 3-(aminomethyl)-6-{3-[4-(trifluoromethyl)phenyl]acryloyl}-2(3H)-benzoxazolones. Turk J Chem. 2021;45:805–18. https://doi.org/10.3906/kim-2101-25.
61. Agrawal PK, Blunden G. Methoxy 13 C NMR Chemical Shift as a Molecular Descriptor in the Structural Analysis of Flavonoids and Other Phenolic Compounds. Nat Prod Commun. 2023;18. https://doi.org/10.1177/1934578X2311710.
62. Alsaygh A, Al-Humaidi J, Al-Najjar I. Synthesis of some new pyridine-2-yl-benzylidene-imines. Int J Org Chem. 2014;4:116–21.
63. Yüksek H, Göksu B, Manap S, Beytur M, Gürsoy Ö, Kol. Synthesis of some new 4-[2-(2-methylbenzoxy)-benzylidenamino]-4, 5-dihydro-1H-1, 2, 4-triazol-5-one derivatives with their antioxidant properties. Int J Chem. 2018;22:1–29.
64. Özbolat G, Yegani AA. In vitro effects of iron chelation of Curcumin Fe (III) complex. Cukurova Med J. 2019;44:947–51. https://doi.org/10.17826/cumj.484672.
65. Kol ÖG, Yüksek H, Manap S, Tokalı FS. Synthesis, characterization and antioxidant activities of novel 1-(morpholine-4-yl-methyl)-3-alkyl (aryl)-4-[4-(dimethylamino)-benzylidenamino]-4, Turkish Chemical Society. 2016;105–118.
66. Kol OG, Yuksek H, Manap S. Synthesis, in vitro antioxidant and antimicrobial activities of some new 2-(3-Alkyl/Aryl-4, 5-dihydro-1H-1, 2, 4-triazol-5-on-4-yl-azomethine) phenyl benzenesulfonate derivatives. J Chem Soc Pak. 2020;42:624–5.
67. Ozdemır G, Alkan M, Yuksek H. Investigation of Biological Properties of New 1-(2, 6-Dimetilmorfolin-4-ylmetil)-3-alkyl (aryl)-4-[3-ethoxy-(4-benzenesulfonyloxy)-benzylidenamino]-4, 5-dihydro-1H-1, 2, 4-triazol-5-ones. The Eurasia Proceedings of Science Technology Engineering and Mathematics. 2018;128–134.
68. Yilmaz Y, Harmankaya A, Manap S, Yuksek H, Kol OG, Alkan M. Antioxidant and Antimicrobial Activities of Some Newly Synthesized 4-[1-(2, 6-Dimethylmorpholin-4-yl-methyl)-3-alkyl (aryl)-4, 5-dihydro-1H-1, 2, 4-triazol-5-on-4-yl-azomethine]-2-methoxyphenyl benzoates. The Eurasia Proceedings of Science Technology Engineering and Mathematics. 2018;72–80.
69. Tahiroğlu V, Gören K, Bağlan M. Silico drug evaluation by molecular docking, ADME studies and DFT calculations of 2-(6-chloro-2-(4-chlorophenyl) imidazo[1,2-a]pyridin-3-yl)-N, N-dipropylacetamide. BMC Pharmacol Toxicol. 2025;26:116. https://doi.org/10.1186/s40360-025-00958-4.
70. Osmaniye D, Ahmad I, Sağlık BN, Levent S, Patel HM, Ozkay Y, Kaplancıklı ZA. Design, synthesis and molecular Docking and ADME studies of novel hydrazone derivatives for ache inhibitory, BBB permeability and antioxidant effects. J Biomol Struct Dyn. 2023;41:9022–38. https://doi.org/10.1080/07391102.2022.2139762.
71. Morak-Młodawska B, Jeleń M, Martula E, Korlacki R. Study of lipophilicity and ADME properties of 1,9-Diazaphenothiazines with anticancer action. Int J Mol Sci. 2023;24:6970. https://doi.org/10.3390/ijms24086970.
72. Ghannay S, Kadri A, Aouadi K. Synthesis, in vitro antimicrobial assessment, and computational investigation of Pharmacokinetic and bioactivity properties of novel trifluoromethylated compounds using in Silico ADME and toxicity prediction tools. Monatshefte Für Chemie - Chem Monthly. 2020;151:267–80. https://doi.org/10.1007/s00706-020-02550-4.
73. Hassan SA, Aziz DM, Kader DA, Rasul SM, Muhamad MA, Muhammedamin AA. Design, synthesis, and computational analysis (molecular docking, DFT, MEP, RDG, ELF) of Diazepine and Oxazepine sulfonamides: biological evaluation for in vitro and in vivo anti-inflammatory, antimicrobial, and cytotoxicity predictions. Mol Diversity. 2025;29:2367–89. https://doi.org/10.1007/s11030-024-10996-5.
74. Boy S, Türkan F, Beytur M, Aras A, Akyıldırım O, Karaman HS, Yüksek H. Synthesis, design, and assessment of novel morpholine-derived Mannich bases as multifunctional agents for the potential enzyme inhibitory properties including Docking study. Bioorg Chem. 2021;107:104524. https://doi.org/10.1016/j.bioorg.2020.104524.
75. Badran A-S, Ibrahim MA. Recyclization of 3-substituted-6,8-dimethylchromones with some heterocyclic enamines: spectroscopic, quantum calculations (HOMO–LUMO, MEP, NLO), biological evaluation, and ADME investigation. J Heterocycl Chem. 2024;61:1224–47. https://doi.org/10.1002/jhet.4827.
76. Khan SA, Asiri AM, Rahman RM, Elroby SA, Aqlan FMS, Wani MY, Sharma K. Multistep synthesis of Fluorine-Substituted pyrazolopyrimidine derivatives with higher antibacterial efficacy based on in vitro molecular Docking and density functional theory. J Heterocycl Chem. 2017;54:3099–107. https://doi.org/10.1002/jhet.2923.

Publisher's note

Springer Nature remains neutral with regard to jurisdictional claims in published maps and institutional affiliations.